Palaeogeography, Palaeoclimatology, Palaeoecology 692 (2026) 113775

Contents lists available at ScienceDirect

Palaeogeography, Palaeoclimatology, Palaeoecology

journal homepage: www.elsevier.com/locate/palaeo

Peatland responses to climate change in the Central Peruvian Andes☆

Yizet E. Huaman-Navarro [a,*], Bruno Turcq [a], Patricia Moreira-Turcq [b], James Apaéstegui [c], Jorge Luis Garcia [d], Isabelle Billy [e], Romina Llanos [f], Bram Willems [g]

[a] Institut de Recherche pour le Développement (IRD) (LOCEAN-IPSL), Sorbonne Université, 75005 Paris, France
[b] Institut de Recherche pour le Développement (IRD)-GET (Géosciences Environnement Toulouse), UMR 5563, France
[c] Instituto Geofísico del Peru, Lima, Peru
[d] Facultad de Ciencias Físicas, Universidad Nacional Mayor de San Marcos, Lima 15081, Peru
[e] Université de Bordeaux, UMR 5805 EPOC (Environnements et Paléoenvironnements Océaniques et Continentaux), Pessac 33615, France
[f] Universidade Federal Fluminense (UFF), Niteroi, Brazil
[g] Universidad Peruana Cayetano Heredia (UPCH), Lima 15086, Peru

ARTICLE INFO

Editor: M Elliot

Keywords:
Andean peatland
Organic matter
Late Holocene
XRF
Compositional data analysis

ABSTRACT

The high central Andes have undergone significant hydroclimatic changes in recent decades, affecting ecosystems through glacier retreat, temperature variations, and shifts in precipitation type (e.g., rain, snow, and hail). Andean peatlands play a crucial role in water regulation and biogeochemical cycles and are highly sensitive to climate change. Here we reconstruct Late Holocene changes in organic matter (OM) accumulation and preservation over the last ~2500 years in a peatland of the south-central Peruvian Andes (4210 m a.s.l.) using the 96-cm APA01 core. We integrate bulk organic geochemistry with continuous X-ray fluorescence (XRF) core scanning, centered log-ratio (clr) transformation, principal component analysis (PCA), and accumulation-rate estimates. A key finding is the close temporal coherence between peat PC1-clr (a proxy for OM dynamics) and the decadal snow accumulation record from Quelccaya Ice Cap, indicating that peat carbon dynamics closely track the regional high-elevation moisture balance. Dry phases such as the Medieval Climate Anomaly (MCA) coincide with reduced OM accumulation, whereas cooler and wetter conditions during the Little Ice Age (LIA) favor enhanced OM preservation. Warming phases, such as the MCA, after LIA, and recent decades, showed high clastic mineral input possibly linked to an increased proportion of rain-to-snow precipitation and land use. These results highlight the sensitivity of Andean peatlands to hydroclimatic variability and underscore the vulnerability of their carbon storage and hydrological functions under ongoing climate change.

1. Introduction

The Andes Mountains have undergone major hydroclimatic changes in recent decades, reflected in surface air temperature and precipitation trends, glacier retreat, runoff variability, and shifts in land cover (Giráldez et al., 2020; Segura et al., 2020). In this context, high Andean peatlands are key ecosystems for water regulation and biogeochemical cycling in the Central Andes (Maldonado et al., 2007; Maldonado-Fonkén, 2014), sustaining higher water availability than surrounding non-peatland areas during drought conditions (Domic et al., 2021). Recent hydrological research highlights the integrative role of Andean peatlands in regulating dry season streamflow under changing climatic conditions, including glacier retreat (Gribbin et al., 2024). Together, these characteristics underscore the sensitivity of high Andean peatland to hydroclimatic variability.

In addition to their hydrological importance, peatlands act as carbon sinks by capturing atmospheric carbon dioxide (CO_2) and storing it in organic deposits for millennia; this function also helps regulate hydrological flow and ensures water availability throughout the year for surrounding and downstream communities (Buytaert et al., 2006; Benavides, 2015; Mosquera et al., 2016; Loisel et al., 2021; Yager et al., 2021; Benavides et al., 2023). Owing to sustained organic matter accumulation, their stratigraphy preserves high-resolution archives of environmental variability, enabling paleoclimatic reconstructions across the tropical and subtropical Andes (e.g., Chimner and Karberg, 2008; Cooper et al., 2010; Hribljan et al., 2014; Schittek et al., 2015,

☆ This article is part of a Special issue entitled: 'SA palaeoclimatology' published in Palaeogeography, Palaeoclimatology, Palaeoecology.

* Corresponding author at: Sorbonne Université Ecole Doctorale des Sciences de l'Environnement d'Ile-de-France (ED 129) UMR-LOCEAN, France.
E-mail address: yizet.huamannavarro@ird.fr (Y.E. Huaman-Navarro).

https://doi.org/10.1016/j.palaeo.2026.113775
Received 19 September 2025; Received in revised form 24 March 2026; Accepted 31 March 2026
Available online 6 April 2026

2016, 2018; Kock et al., 2019a; Benfield et al., 2021; Perez and Loisel, 2023).

The development and persistence of peatlands depend strongly on the interaction between climate, hydrology, and geomorphic processes. In high-Andean peatlands, local hydrological and thermal conditions regulate the balance between organic matter production and decomposition, thereby controlling carbon accumulation rates (CAR) (Chimner and Karberg, 2008; Hribljan et al., 2014, 2016). Climate variability also influences sediment transport through precipitation-driven runoff and eolian deposition, thereby affecting soil physical properties and mineral accumulation rates (MAR) (Schittek, 2012; Kylander et al., 2018). These hydro-geomorphic interactions are particularly important because saturated conditions and mineral inputs may act together to limit microbial decay and enhance organic matter preservation (McCarter et al., 2020; Oyague et al., 2022).

Over the past two decades, research has documented substantial peat deposits and/or rapid accumulation rates at various high Andean sites (e.g., Earle et al., 2003; Benfield et al., 2021; Hribljan et al., 2024). These peat forming wetlands are critical landscape features in the Andes, providing essential ecosystem services such as forage for camelids managed by indigenous pastoralists, as well as carbon sequestration and water storage (Verzijl and Quispe, 2013; Yager et al., 2021; Monge-Salazar et al., 2022; Martínez-Amigo and Jaramillo, 2024). However, climate change is intensifying precipitation irregularities, disrupting the hydrological balance, and raising fire risk and carbon release from high Andean peatlands (Loisel et al., 2021; Perez and Loisel, 2023). Altered rainfall regimes may lead to peatland drying, increasing the risk of fires and the release of large amounts of stored carbon, thereby contributing to global warming (Loisel et al., 2021). Moreover, rising temperatures and climate variability accelerate organic matter decomposition, reducing their ability to function as long-term carbon sinks (Gutiérrez-Salazar and Medrano-Vizcaíno, 2019; Nikonova et al., 2023).

Assessing the effects of future climate change on peatlands requires studying their historical variability and responses to past climatic shifts over millennia. X-ray fluorescence (XRF) core scanning provides continuous, high resolution, semi-quantitative profiles of elemental intensities (counts per second, cps) along sediment and peat sequences and has become a widely used tool for paleoclimate reconstructions (Kern et al., 2019; Kock et al., 2019b; Longman et al., 2019; Lücke et al., 2022). In organic rich archives, XRF core scanning datasets, which typically include major, minor and trace elements (Al, Si, S, K, Ca, Ti, Mn, Fe, Ni, Zn, Br, Rb, Sr, Zr, and Pb), are widely applied to infer past environmental and climatic conditions, with numerous elemental ratios serving as indicators of the variability of processes depending on the study context and location (Weltje and Tjallingii, 2008; McKinley et al., 2018; Kern et al., 2019; Lee et al., 2019; Longman et al., 2019; Bábek et al., 2022). Variations in lithogenic elements (e.g., Al, K, Ti, Rb, Zr) commonly reflect detrital minerogenic flux linked to catchment erosion and hydrodynamics. This approach has been successfully applied in Andean peatlands to differentiate between clastic dominated layers, indicative of increased runoff or eolian input, and periods of organic matter accumulation (Schittek et al., 2015; Kock et al., 2019a; Lücke et al., 2022). Ratios such as S/Ti are applied in this study, to explore organic matter dynamics and redox-sensitive processes in organic-rich, waterlogged environments, where sulphur is preferentially associated with organic matter under reducing conditions (Fennell and Bentley, 1998; Tribovillard et al., 2006), whereas titanium represents a conservative detrital input. When interpreted in combination with independent organic proxies, S/Ti can therefore provide insights into variations in organic matter preservation rather than serving as a proxy for organic matter content. Likewise, the Zr/Ti ratio is widely used as an indicator of erosion intensity and grain-size variability within a catchment, since zirconium is concentrated in heavy minerals resistant to weathering and transport, while titanium is primarily hosted in fine-grained clay minerals and oxides (Rothwell and Croudace, 2015).

Against this broader regional framework, site specific conditions are expected to strongly modulate peatland responses to climate variability. In some Andean regions, peatlands receive hydrological inputs from glacial meltwater (Cuesta et al., 2019). In the study area investigated here, however, glaciers have disappeared, and moisture inputs now depend exclusively on precipitation (rain, snow, and hail) and groundwater storage. In addition, the Central Andes are characterized by marked daily and seasonal temperature oscillations and frequent frost events (SENAMHI, 2020). These conditions provide an important local context for interpreting the environmental history recorded in the peat sequence.

This study reconstructs the environmental history of a high Andean peatland in Peru by analyzing the chemical elemental composition obtained through clr-transformed XRF peat core scanning data and bulk organic geochemical characteristics. By situating these inferred phases within the broader context of regional paleoclimate records, we aim to identify the historical responses of these ecosystems to climatic variability.

2. Study area

The study area is in the central region of the Peruvian Andes (Fig. 1). This section of the Andes water network drains into the Atlantic Ocean. According to the SENAMHI (Servicio Nacional de Meteorología e Hidrología del Perú) and the Climate Classification Map of Peru (SENAMHI, 2020) the study area presents a semi-dry zone classification, characterized by being rainy with a moisture deficiency and cold

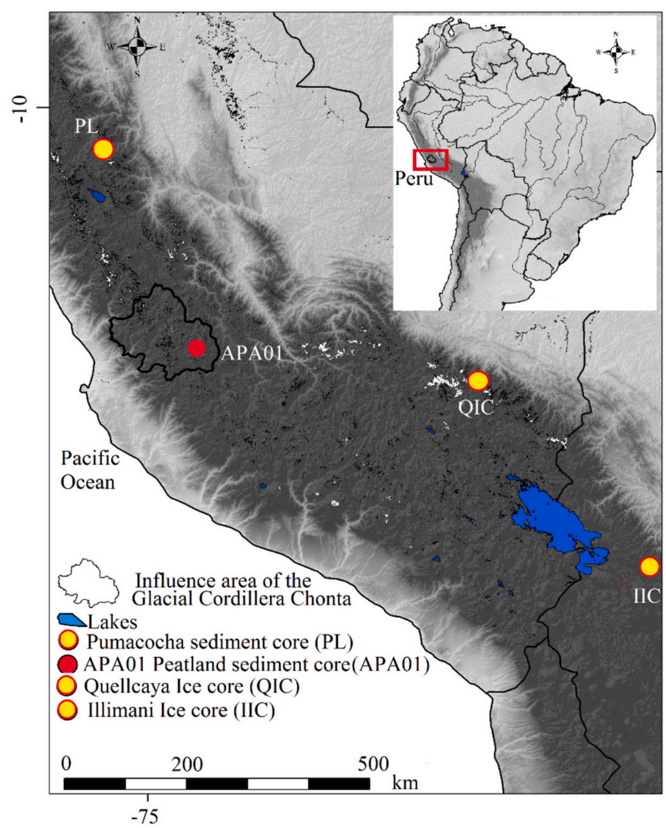

Fig. 1. Location of the study area and other paleoclimate records cited. The bold black line delineates the zone of influence (hydro-glaciological drainage domain) of the Cordillera de Chonta as defined by INAIGEM (2018). The red circle indicates the location where the APA01 peat core was collected. Yellow circles represent the Pumacocha Lake record (PL) (Bird et al., 2011), Quelccaya ice core (QIC) (Thompson et al., 2013) and Illimani ice core (IIC) (Kellerhals et al., 2010) locations, respectively. (For interpretation of the references to colour in this figure legend, the reader is referred to the web version of this article.)

temperatures occurring primarily from April to September, with the coldest and most frequent conditions in June and July. At these elevations (>3600 m a.s.l.), precipitation frequently occurs as solid forms (snow and hail), particularly associated with seasonal frost events (SENAMHI, 2020). Rainfall is concentrated in the central-eastern part of the mountain range, with an annual average of 700 to 800 mm, mainly occurring from December to March following the South American Monsoon System (SAMS). The annual average minimum air temperature ranges between −3 °C and − 1 °C, and the annual average maximum air temperature is 13–15 °C. The glaciers in this part of the mountain range have declined significantly since 1962, from 17.85 km^2 to only 0.37 km^2 in 2020. The reduction in glacier area has been progressive: from 17.85 km^2 in 1962 to 9.35 km^2 in 1997, before dropping drastically to 1.4 km^2 in 2009 and reaching 0.38 km^2 in 2016 (INAIGEM, 2018; INAIGEM, 2023). Currently, there is no glacier in the peatland catchment studied (APA01), which rises to 4912 m a.s.l. However, there is a rock glacier on Portuguesa Peak, located across the Apacheta River, which extends from 4800 to 5120 m a.s.l. (Swann Zerathe, personal communication). It is quite possible that this type of glacier was present in the study area in the past. The predominant geology around the APA01 sampling area, obtained from GEOCATMIN, the online platform from the INGEMMET (Geological, Mining and Metallurgical Geological Institute), includes the Apacheta Formation and Chahuarma Formation, composed of andesitic lava flows, breccias, domes, and andesitic to basaltic lava flows and rhyolitic tuffs in thick layers, respectively.

Our study area is located at the headwaters of the Apacheta River basin, home to several water sources that feed a type of high Andean wetland characterized by peat formation. These peatlands locally referred to as "bofedales" throughout the Central Andes (e.g., Peru, Bolivia, northern Chile, and northwestern Argentina), are hybrid terrestrial-aquatic ecosystems that include both peat-forming environments and wet meadows and are strongly influenced by local hydrology and valley scale conditions (Polk et al., 2019). In this region, *Distichia muscoides* (Juncaceae) is predominant in cushion peatland, and is present on most high elevation peatlands in the central Peruvian Andes (Skrzypek et al., 2011; Schittek, 2012; Schittek et al., 2015; Polk et al., 2017, 2019; King et al., 2021). Further vascular plant species, which are typically found in bofedales of the Apacheta region, are *Plantago tubulosa, Aciachne pulvinata, Scirpus rigidus, Calamagrostis rigescens, Calamagrostis* spp., *Hypochaeris sessiliflora,* and *Hypsela reniformis* (Polk et al., 2019). The *Distichia* cushions can grow so densely that it forms extensive, stable mats, varying in shape from almost flat to hemispherical, where new shoots develop at the surface, while older basal tissues undergo senescence, are progressively buried, and are preserved under waterlogged conditions, contributing to peat accumulation (Cooper et al., 2010, 2018; Hribljan et al., 2014; Oyague, 2020; Benfield et al., 2021). The local catchment area of the APA01 peatland, defined as the immediate drainage area supplying water and sediment directly to the site, covers approximately 3.3 km^2, where *Distichia muscoides* cushions are surrounded by small, shallow water pools, typical of this ecosystem type.

3. Materials and methods

In April 2015, core APA01 was extracted at an elevation of 4210 m a.s.l., at coordinates 13° 21′ 4.61" S and 74° 39′ 31.75" W (Fig. 1). The APA01 core was collected manually using an 8 cm diameter PVC tube. The PVC tubes were pushed into the peat by hand pushing. A PVC plug was inserted into the top of the tube and secured with adhesive tape to create vacuum and the core was pulled out using a rope and a Prussik knot. The core has a recovered length of 96 cm. The total peat thickness at this site remains unknown. Additional parallel cores were collected across the peatland; however, detailed analysis focused on the APA01 core. The pH, conductivity, and dissolved oxygen of the waterhole in the peat were measured using a Hach Portable HQ40D model. The values obtained were pH 5.93, electrical conductivity (EC) 45.4 μS cm^{-1}, and dissolved oxygen (DO) 16.39 mg L^{-1}, respectively.

The core PVC tube was cut using a circular saw, described, and sampled in the laboratory. The lithological description was carried out immediately after opening of the core, to avoid possible alterations due to the oxidation of the sediment. The sedimentological and macroscopic characteristics (e.g., texture) were described by visual inspection, while sediment colors were determined using Munsell Soil Colour Charts. Additionally, the composition of the organic matter present in the peat core (e.g., diatoms, spicules and amorphous organic matter) was observed on raw sediment slides under an optical microscope.

Two parallel aluminum U-channels were employed to collected peat samples from each side of the core section immediately after opening. One channel was subsampled at 1-cm resolution to determine the bulk density and water content from wet and dry mass measurements, while the second channel was kept intact for XRF core scanner.

Radiocarbon measurements (^{14}C) were performed on eight bulk peat samples using ARTEMIS accelerator mass spectrometry (AMS) system based on a 3MV Pelletron from National Electrostatics Corporation (NEC, Middleton, Wisconsin, USA) at the Laboratoire de Mesure du Carbone 14 (LMC14) - UMS 2572 (CEA/DSM, CNRS, IRD, IRSN – Ministère de la Culture et de la Communication). Radiocarbon ages were calibrated, with ranges calculated using OXCAL 4.4 (Bronk Ramsey, 2020). An age-depth model was developed using the Clam 2.4 (Blaauw, 2010) package in R software and the SHCal20 (Hogg et al., 2020) and to ensure precision in the recent part of the record, three of these samples were processed as post-bomb dates. These modern samples were analyzed using percent Modern Carbon (pMC) values and calibrated against the post-bomb Bomb21SH3 (Hua et al., 2022) calibration curves. Radiocarbon dating was performed on bulk peat samples, an approach commonly applied in high Andean peatland archives (e.g., Schittek et al., 2016; Benfield et al., 2021; Hribljan et al., 2024), where peat is dominated by in situ vertical accretion of root and shoot biomass (Cooper et al., 2010), resulting in a matrix that is expected to be largely autochthonous.

Wet volume and dry weight data from APA01 were used to obtain the bulk density (g/cm^3). Organic matter content was determined by loss on ignition (LOI) on a dry weight basis, by ashing subsamples for 5 h at 550 °C after drying overnight at 105 °C (Wang et al., 2013). Mineral content was estimated by subtracting the weight of organic matter lost after combustion from the total weight of the material before combustion. Determinations of total organic carbon (TOC), total nitrogen (TN) and stable isotopic carbon (δ13C) content were performed using a CHN analyzer (FISIONS NA-2000) connected to an isotope ratio mass spectrometer, (Micromass Optima) at University of California, Davis, CA, USA. (https://stableisotopefacility.ucdavis.edu/carbon-and-nitrogen-solids).

Core APA01 was X-ray analyzed using SCOPIX equipment at the EPOC laboratory (Environnements et Paléoenvironnements Océaniques et Continentaux) at the University of Bordeaux, France. The SCOPIX has a microfocus X-ray source of 130 KV and 0.3 mA. Elemental analysis by X-ray fluorescence (XRF) Spectrometry is a non-destructive technique that allows for continuous, relatively fast, and high-resolution measurement of X-ray fluorescence of several chemical elements present in sediments (Jansen et al., 1998; Croudace et al., 2006; Löwemark et al., 2011; Croudace et al., 2019b). In this study, the resolution was set at 5 mm. From XRF analysis of APA01, 15 elements (expressed in counts per second) were obtained: Al, Si, S, K, Ca, Ti, Zn, Mn, Fe, Ni, Br, Rb, Sr, Zr, and Pb. Principal component analysis (PCA) was carried out using the software package PAST 4.15 first with the number of counts of each element. However, the relationship between number of counts and concentrations is often non-linear, due to (1) the matrix effect (Löwemark et al., 2011; Weltje et al., 2015) which reflects interactions between fluorescent elements, which absorb incoming radiation but also increase fluorescence emission, and (2) the ratio between fluorescent and non-fluorescent elements in the sample. In our case, these non-fluorescent elements are a large amount of organic matter and the water filling the peat's high porosity. To reduce these two effects, Weltje et al. (2015) suggested using the centered log-ratio of fluorescence intensity.

Moreover, statistical analysis of concentration data can often display spurious correlations and face issues related to the closure of datasets, as the sum of individual elements is constrained to a constant sum (Aitchison, 1982; Aitchison and Greenacre, 2002; Filzmoser et al., 2009). By applying clr-transformation, these issues are mitigated, allowing for more accurate and reliable interpretations of geochemical trends and relationships (Grunsky and Caritat, 2020; L. Wang et al., 2021; Banríon et al., 2023).

To mitigate non-linear matrix effects and constant-sum constraints, multivariate statistical analysis was applied after a centered log-ratio (clr) transformation using PAST 4.15 software (Hammer et al., 2001). The clr transformation is given by eq. 1 (Aitchison, 1982; Aitchison and Greenacre, 2002):

$$clr(x) = \left[\frac{\ln x_1}{g(x)}, \ldots, \frac{\ln x_N}{g(x)}\right] \quad (1)$$

Where *g(x)* is the geometric mean of the data vector. This is equivalent to a simple log transformation followed by subtraction of the mean (Aitchison, 1982; Filzmoser et al., 2009). This simple transformation provides a reliable basis for statistical analysis of XRF core scan data, unlike element count intensities or simple element ratios and is the best proxy for element concentration (Weltje and Tjallingii, 2008; Weltje et al., 2015). The correlation matrix was calculated by hierarchical clustering analysis (HCA) using the classical multivariate cluster function of the PAST 4.15 software. The hierarchical clustering plot of the clr-transformation resulted in a cophenetic correlation coefficient of 0.88.

Principal component analysis was applied to the XRF dataset to identify major patterns of multivariate variability and elemental covariation along the core. Samples were grouped into a limited number of phases, represented by different colors in the PCA-clr plot. These phases were defined based on changes in the raw XRF chemical elements profiles and correspond to intervals with distinct geochemical behaviors.

4. Results

4.1. Lithological description and chronology

Core APA01 reflects the dominance of organic clay and plant debris throughout its 96 cm length. Plant remains are more abundant near the surface and decrease gradually with depth, while organic clay content becomes more dominant in the basal sections. Across the profile, hues consistently fall within the 5YR range, suggesting relatively stable redox conditions during peat formation. From the base (96 cm) up to 38 cm depth, the peat core consists of organic clay ranging from 5YR 2.5/2 (Dark Reddish Brown) to 5YR 3/3 (Dark Reddish Brown), with alternating hues. Between 38 and 31 cm, the coloration remains 5YR 3/3 (Dark Reddish Brown); this layer is composed of organic clay containing millimeter sized root fragments, followed by a section from 31 to 24 cm characterized by black organic clay (5YR 2.5/1) with fewer plant remains. From 24 to 6 cm, dark reddish brown organic clay (5YR 3/2) predominates, with an increased abundance of centimeter sized plant remains, leading to the surface layer (6–0 cm), which is composed of black organic clay (5YR 2.5/1) with abundant centimeter-sized plant debris. Overall, the peat composition reveals alternating layers of organic rich sediment providing insights into the shifts in peat forming conditions through to surface processes.

Microscopic analysis of the sediments mainly allowed us to observe the composition of the organic matter present in the core. From the base of the core to approximately 40 cm in depth, the sediments can be characterized as devoid of diatoms due to the very low concentration of valves. From 40 cm to the surface, a great wealth of diatoms and amorphous organic matter is found. The most representative diatoms were from the genera *Pinnularia, Synedra*, and *Cymbella.*

The age–depth model was developed using eight radiocarbon dates (Table 1), obtained from bulk peat samples, yielding a basal ^{14}C age of approximately 2500 calibrated years BP (450 years BCE). The resulting model shows a stratigraphic consistency with no identified age reversals throughout the 96 cm profile (Fig. 2) and wo distinct accumulation phases were identified. The boundary between Phase 1 and Phase 2 was defined at the inflection point of the accumulation profile, where a clear change in slope marks a distinct shift in accumulation rate. Consequently, lower phase from 96 to 38 cm, characterized by a nearly constant accumulation rate of 0.027 cm yr^{-1}, and an upper phase from 37 cm to the surface, showing a substantially faster rate of 0.3 cm yr^{-1} (Fig. 2). The bulk density of APA01 varies from 0.069 g cm^{-3} to 0.319 g cm^{-3}, with an average of 0.172 g cm^{-3}. Lower density was found near the surface (Fig. 3).

4.2. Geochemical variability of the APA01 core

4.2.1. Organic geochemistry

The APA01 core exhibits clear variations in its organic geochemical profiles along its 96 cm length (Fig. 3), reflecting shifts in organic matter production and preservation conditions. TOC content varies substantially between 11.93% and 44.01% (Fig. 3), with a mean of 31.34% and moderate dispersion. The carbon-to-nitrogen (C/N) ratios range from 6.65 to 18.78 (mean: 13.27), while $\delta^{13}C$ values remain relatively homogeneous, spanning from −28.50 ‰ to −25.40 ‰ (mean: −26.43 ‰). Notably, the highest TOC concentration (44.01%) is recorded at ~30 cm, where the C/N ratio also peaks at 18.58.

The lowest $\delta^{13}C$ value (−28.50 ‰) occurs at ~8 cm, coinciding with a low TOC (18.73%) and the lowest C/N ratio (7.94). Between ~6 and ~24 cm, TOC remains relatively stable and elevated, ranging from 24.96% to 31.51%, with consistent C/N values and moderate densities. Between approximately 37–38 cm, the core exhibits the highest bulk density (0.314 g cm^{-3}), a low total organic carbon (TOC) value (15.73%), and a moderate carbon to nitrogen (C/N) ratio of 12.02. Similarly, the ~84 cm depth stands out for exhibiting both a high C/N ratio (18.78) and TOC (39.54%) within a denser layer (0.215 g cm^{-3}).

4.2.2. X-ray Fluorescence (XRF)

The XRF scan of core APA01 allows the determination of the main geochemical variations in the peat core which is shown in Fig. 4 as counts per second (cps). The strong similarity in the trends of K, Zr, Ti, and Rb suggests that these elements are primarily related to processes associated with terrigenous inputs. The two prominent events observed at 60–58 cm and 36–34 cm depths may indicate episodes of increased clastic inputs or changes in the peatland environment. Sr and Ca both show a tendency to decrease toward the top of the core, as does TOC. Si, although naturally ubiquitous in terrigenous sediments, does not show the same tendency as K, Zr, Ti and Rb. The differences between the Si curve and those of the terrigenous elements implies the contribution of biogenic Si. It increases toward the top of the core, showing three marked peaks at 60–58 cm, 36–34 cm, and 17 cm.

4.3. Multivariate patterns in X-ray fluorescence data

Principal component analysis (PCA) was applied to both the raw XRF data and the clr-transformed data, offering insights into the primary variability of geochemical components related to accumulation processes in the APA01 peat core. In the PCA of the raw XRF data (Fig. 5a), PC1 and PC2 account for 31.7% and 25.4% of the total variance (Fig.S3), respectively. Notably, almost all elements appear on the positive side of PC1, except for Mn, Ni, and Br. This observation suggests that factors not directly measured by fluorescence contribute to the observed variability. In organic-rich peat deposits such as APA01, variations in the amount of

Table 1
Radiocarbon ages of core APA01. Calibrated age ranges were calculated using OxCal 4.4 and SHcal20, and for the first 3 dates Bomb21SH3 was used.

Code	Depth (cm)	Material	$\Delta^{13}C$	pMC*	Age ^{14}C yr BP	Calibrated OxCal4.4 yr CE
SacA43147	2–3	Peat	−29.7	106.91 ± 0.32	After 1950	(2005) **2006** (2007)
SacA43149	14–15	Peat	−31.9	136.97 ± 0.42	After 1950	(1969) **1981** (1997)
SacA43150	25.5–27	Peat	−26.9	102.86 ± 0.31	After 1950	(1938) **1963** (1976)
SacA43151	32.5–33	Peat	−28.9	98.58 ± 0.31	115 ± 30	(1800) **1877** (1939)
SacA43152	50–51	Peat	−27.1	95.91 ± 0.31	335 ± 30	(1478) **1501** (1637)
SacA43153	62–63	Peat	−30.6	87.43 ± 0.29	1080 ± 30	(941) **975** (1022)
SacA43154	79–80	Peat	−27.5	78.73 ± 0.26	1920 ± 30	(57) **151** (209)
SacA43155	95–96	Peat	−25.8	74.30 ± 0.26	2385 ± 30	(−541) **-507** (−394)

* percent Modern Carbon.

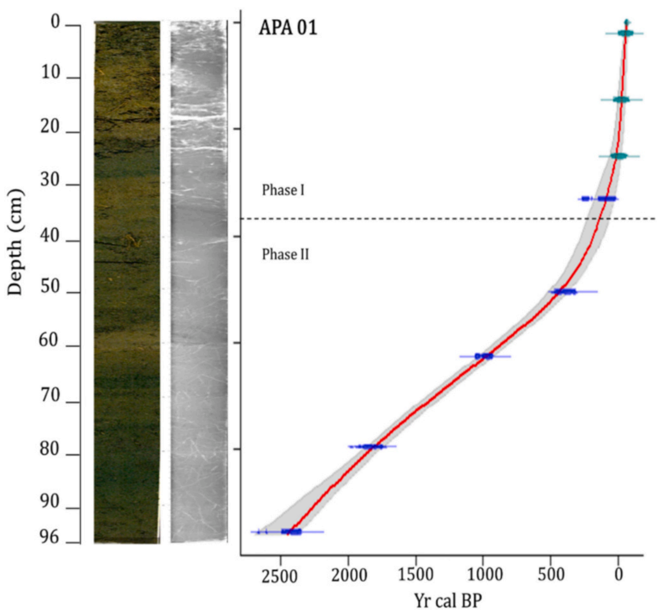

Fig. 2. Stratigraphy and chronological model of APA01 peat core. Left panel, photograph of the APA01 sediment core. The middle panel presents the radiography image of APA01 core. The right panel presents the chronological model with 8 ^{14}C dates. The dates in green represent post-bomb dates, and they are divided into two well-marked sections. (For interpretation of the references to colour in this figure legend, the reader is referred to the web version of this article.)

organic matter (OM) and pore-water filling can strongly influence XRF signal intensities, leading to matrix effects and distorted elemental relationships (Rothwell and Croudace, 2015; Lee et al., 2019). This likely explains the clustering of most elements on the positive side of PC1 in the raw-data PCA.

Multivariate analysis was then repeated on the clr-transformed dataset. This clr transformation compares the fluorescence signal of each element relative to the others by using the geometric mean as the denominator, thereby minimizing the proportion effect. As a result, the subsequent multivariate analysis can describe the concentrations of the APA01 elements in a more homogeneous and standardized way. Fig. 5b illustrates this improvement: the PCA on clr-transformed data shows a more balanced distribution of fluorescent elements in the PC1-clr and PC2-clr space, which now account for 53.6% and 35.1% of the total variance (Fig. S4), respectively. In this analysis, Ca, S, and Sr are positively correlated along PC1-clr, while Ti, Zr, and Rb are positively correlated along PC2-clr. The negative correlation of Si with both PC1-clr and PC2-clr likely reflects the combined influence of clastic and biogenic materials. Four geochemical phases were identified in core APA01 using XRF elemental data. These phases correspond to the intervals 1900 to 2015 CE, 1550–1890 CE, 900–1325 CE, 507 BCE to 900 CE. They are shown as colored groups in the PCA-clr biplot (Fig. 5b).

5. Discussion

5.1. Interpretation of XRF data

The principal components analysis (PCA) of the XRF-clr records (Fig. 5b) shows that PC1-clr and PC2-clr together explain 88.8% of the total variance, a higher percentage than the previous PC analysis, indicating that the variability linked to external components (e.g., water, organic matter, matrix effect) have been at least partly eliminated by the transformation. In this new PCA-clr, the PC1-clr is influenced by the group of S, Ca, and Sr elements. In Fig. 6a, the PC1-clr curve is compared with the OM % and TOC % contents. PC1-clr shows a coherent covariation with both organic matter proxies, consistent with its dominant positive loadings on S, Ca, and Sr and negative loadings on clastic elements such as Al, K, and Rb (Table S1). This pattern indicates that PC1-clr primarily reflects variations in organic matter accumulation and preservation relative to mineral inputs in this acidic, organic rich environment.

Accordingly, the log(S/Ti) ratio follows a similar pattern to PC1-clr (Fig. 6a, see also Fig. S5a), supporting its use as a proxy for organic matter dynamics (Moreno et al., 2007). In this kind of cores, the S/Ti ratio can vary due to factors such as the intensity of organic matter production and decomposition in the peatland, the presence of oxygen in the water, the amount of organic material available for accumulation, and the water temperature (Moreno et al., 2007). In general, when the S/Ti ratio is high, it is interpreted to mean that the production of organic matter has been high. This is because sulphur is concentrated in the organic material produced during photosynthesis (Tribovillard et al., 2006). Therefore, the S/Ti ratio can be used to infer the variability of the production and decomposition of organic matter in the peatland's past, and consequently, the influence of environmental factors on that variability (Fennell and Bentley, 1998). In addition, the S/Ti ratio can also be sensitive to the presence of oxygen in the water. When there is sufficient oxygen in the water, sulphur is oxidized and removed in the form of sulphate (SO_4), which causes the S/Ti ratio to be low. In contrast, when the water is deficient in oxygen, sulphur is not oxidized and is deposited in the peatland, which increases the S/Ti ratio (Dickens, 2011). The consistent covariation between log(S/Ti), PC1-clr, and organic matter content suggests a close coupling between organic matter concentration and low oxygenation conditions, consistent with oxygen consumption during organic matter degradation. PC2-clr is, in part, influenced by the opposition between silicon and the elements associated with organic matter such as S, Sr, Ca (Fig. 5b). Elements typically found in clastic sediments such as titanium (Ti), zirconium (Zr), potassium (K), and rubidium (Rb) (Rothwell and Croudace, 2015) which showed the highest loadings on PC1 of the raw dataset prior to clr-transformation, are distributed over the negative values of PC1-clr and the positive values of PC2-clr. Positive PC2-clr values are therefore influenced by the variability of clastic inputs.

Silicon (Si), although present in all siliciclastic material, does not

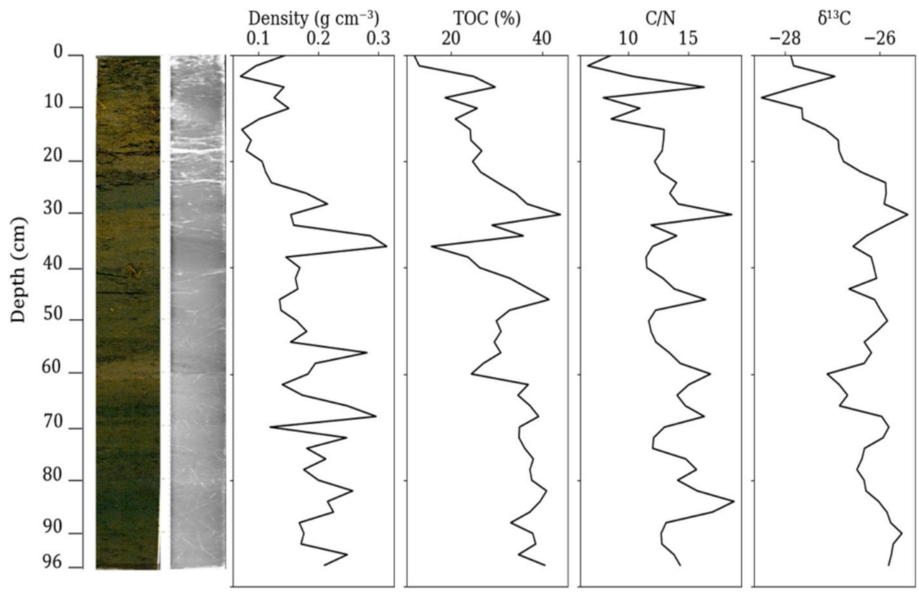

Fig. 3. Profiles of the APA01 peat core showing (from left to right) a core photograph, X-ray radiograph, bulk density (g cm^{-3}), total organic carbon (TOC, %), C/N ratio, and stable carbon isotopic composition (δ^{13}C, ‰ VPDB) plotted against depth.

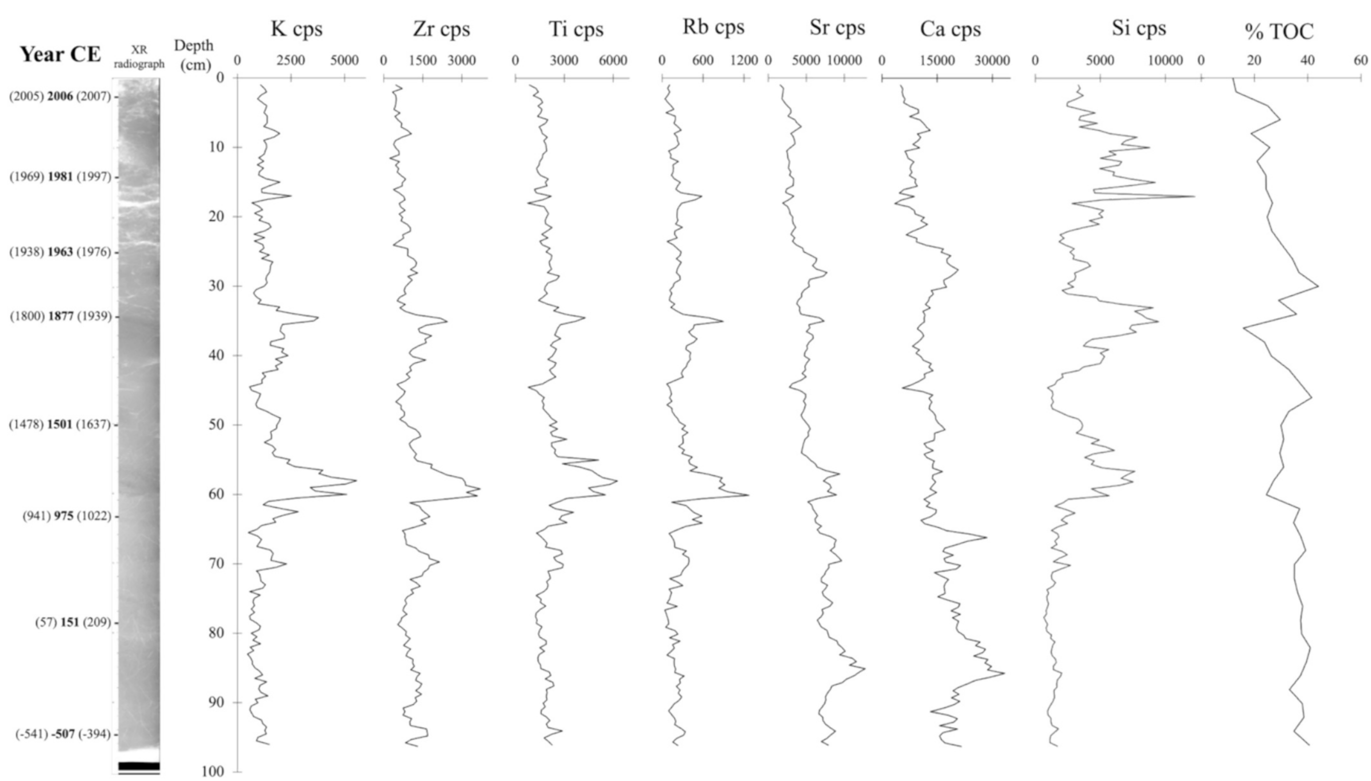

Fig. 4. Profiles of X-ray fluorescence (XRF) elemental intensities for peat core APA01, including K, Zr, Ti, Rb, Sr, Ca, and Si, expressed as count per second (cps), and Total Organic Carbon (%TOC). The vertical axis indicates depth (cm), with the corresponding calibrated age (Year CE) derived from the age-depth model. The X-ray radiograph of peat core section is shown on the left. Each panel displays the corresponding chemical elemental plotted against depth.

follow the same patterns as clastic-derived elements, as it is negatively related with PC2-clr. This may indicate that some of the Si present in these peatlands is not only derived from clastic sediment inputs but also have a biogenic origin, as observed with diatoms distribution in the peat core. In high altitude Andean peatland, studies have documented that diatoms (siliceous microalgae) present in the peat can be a significant source of biogenic silica (King et al., 2021). These microalgae incorporate dissolved silica into their frustules, and their accumulation in peat sediments could explain the presence of biogenic Si (Kokfelt et al., 2009; Gaiser and Rühland, 2010; Smol and Stoermer, 2010; Carballeira and Pontevedra-Pombal, 2020; King et al., 2021). In our study, we observed an inverse relationship, during certain periods, between TOC and silicon (Fig. S2). An increase in OM degradation could result in a relative enrichment of biogenic silica, which may explain the observed opposition between silicon and elements associated with TOC values. This process has been documented in peat records, where the selective

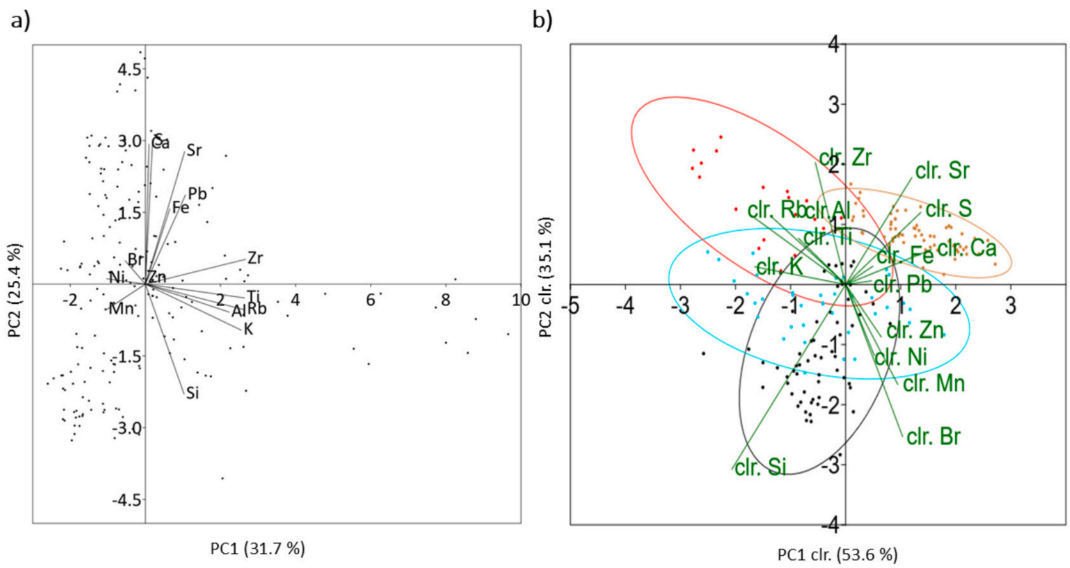

Fig. 5. Principal component analysis (PCA) biplots of X-ray fluorescence (XRF) data from the APA01 peat core. (a) PCA based on raw elemental intensities (counts per second), showing the distribution of elements and sample scores along PC1 and PC2. (b) PCA based on centered log-ratio (clr) transformed data, showing the distribution of elements and samples along PC1 clr. and PC2 clr. The percentage of variance explained by each principal component is indicated on the axes. Sample points are colored by approximate time interval: ~1900 to 2015 CE (black), ~1550–1890 CE (light blue), ~900–1325 CE (red), and ~ 507 BCE to 900 CE (brown). (For interpretation of the references to colour in this figure legend, the reader is referred to the web version of this article.)

preservation of siliceous microfossils, such as diatom frustules, contributes to silicon accumulation as organic matter decomposes (Carballeira and Pontevedra-Pombal, 2020; King et al., 2021). We propose the use of the log(Si/S) ratio as a complementary proxy to assess organic matter degradation in high Andean peatland.

In addition to Si dynamics, zirconium (Zr) is also an important element contributing to PC2-clr variability. This element is found in zircon minerals, which are very resistant to weathering (Longman et al., 2019). As a result, Zr tends to concentrate in the peat coarse fraction. Variations in Zr would indicate a variability in grain size along the core (Croudace et al., 2019a). The Zr/Ti ratio is widely used as an indicator of erosion intensity in a watershed since Zr is found in heavy minerals that are more difficult to be eroded and transported by run-off, while Ti is found in clay minerals or Titanium oxides produced from the weathering of rocks and easily removed by run-off (Bain, 1976; Croudace et al., 2019b). In ombrotrophic peatlands, Zr may also serve as an indicator of fine-grained eolian dust deposition under dry and windy conditions (Croudace et al., 2019a). However, in the minerotrophic APA01 peatland, Zr variability is primarily interpreted as reflecting changes in local detrital inputs and erosion dynamics within the catchment.

The red curve in Fig. 6b represents the second principal component (PC2-clr), which explains 35.1% of the variance. PC2-clr captures temporal changes in geochemical and sedimentary conditions of the peat core. Its values fluctuate markedly between 1560 and 2000 CE (Fig. S1), with a shift toward more negative scores after ~1900 CE ±100. This shift consists of changes in climatic forcing and depositional conditions. The late-20th-century decline in PC2-clr coincides with reduced organic-matter accumulation and greater clastic input. We plot log(Si/S) and log (Zr/Ti) alongside PC2-clr in Fig. 6b, consistent with relations shows in Fig. S5b-c. The Si/S ratio constrains organic-matter preservation versus degradation and complements the PC1-clr signal. Comparing log(Si/S) with PC1-clr in Figs. 6a–b shows that intervals of high PC1-clr (high OM) tend to coincide with low log(Si/S), indicating limited OM degradation.

In Fig. 6c we show carbon accumulation rate (CAR) and mineral accumulation rate (MAR), which trace accumulation dynamics in this high-Andean peatland. From 507 BCE ±100 to 1565 CE ± 100 both CAR and MAR remain low. Given that organic carbon is ~62% of organic matter, CAR would be about twice as high as MAR under OM-rich conditions. Comparing log(Si/S) with PC1-clr in Figs. 6a–b and S1a–b indicates that intervals with high PC1-clr and low log(Si/S) coincide with lower OM degradation and more reducing conditions reflected by high log(S/Ti). Periods when CAR exceeds MAR (e.g., ~100 BCE–100 CE and ~ 700–800 CE; Fig. 6c) show low Si/S, consistent with limited OM degradation. In contrast, ~1100–1300 CE and ~ 1750–1850 CE, when MAR > CAR, display high Si/S, implying stronger OM degradation and enhanced clastic deposition.

A focus on the period covering from 1570 CE ±100 through the most recent part of the record is marked by an increase in both CAR and MAR (Fig. S1). During this period, the log(Si/S) is variable with a tendency to increase while the CAR is increasing exponentially. This suggests that the increase in organic matter accumulation can be attributed to organic matter production instead of less organic matter degradation. However, log (Zr/Ti), which is a marker of granulometry and soil erosion, became highly variable during this period, indicating higher hydrodynamics in this environment corresponding to the higher supply of mineral material. These conditions probably also produce a higher supply of nutrients that sustain the higher primary productivity.

In conclusion, the reconstructed geochemical record provides significant insights into palaeohydrological conditions and peat accumulation process in this high Andean ecosystem. By integrating clr-transformation of XRF data with independent organic matter measurements, the analysis allows the isolation of geochemical signals linked to organic matter from detrital inputs, enabling a process-based interpretation of peatland responses to past hydroclimatic variability in Central Andes. The results further reveal relationships between organic matter content and geochemical proxies of oxygenation and erosion intensity, highlighting how hydrological conditions and catchment processes jointly modulate the balance between peat production and decomposition in this high Andean archive.

5.2. *Climate reconstruction*

5.2.1. *Influence of global climate on Central Andes*

In the Andes, numerous paleoclimate reconstructions covering the last millennium have been developed using a wide range of archives, including glacial ice cores, moraines, lake sediment cores, speleothems, and tree rings (e.g. Liu et al., 2005; Liu et al., 2007; Vuille et al., 2008; Vimeux et al., 2009; Bird et al., 2011; Rabatel et al., 2013; Thompson

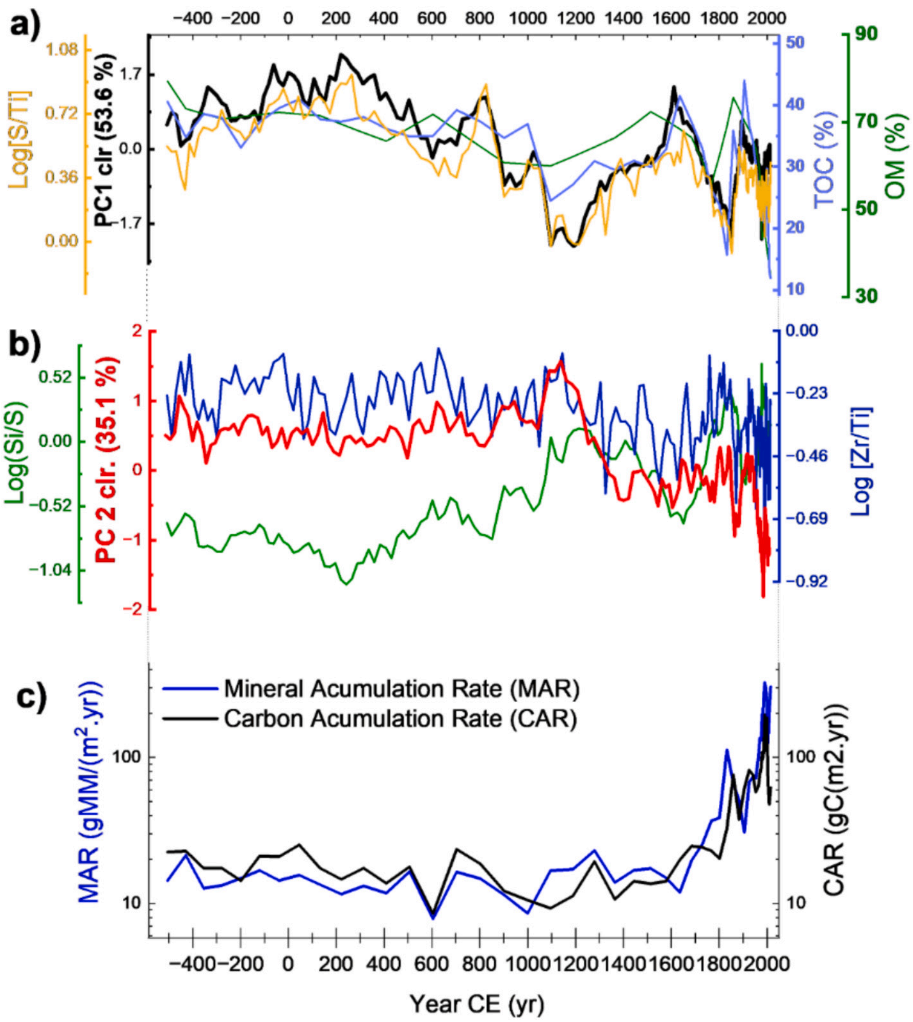

Fig. 6. Temporal evolution of PC1-clr and PC2-clr of core APA01: a) The PC1-clr curve is compared with log(S/Ti), TOC (Total Organic Carbon %), and OM (Organic Matter %); b) The PC2-clr curve is compared with log(Zr/Ti) and log(Si/S); c) The temporal evolution of the mineral accumulation rate (MAR) and the carbon accumulation rate (CAR), both representing the accumulation dynamics over the last 2500 years in APA01 peat core.

et al., 2013; Apaéstegui et al., 2014; Schittek et al., 2018; Vuille et al., 2018; Kock et al., 2019a; Ancapichún et al., 2021; Schittek et al., 2025). Within this comparative framework, the APA01 peat core record provides a complementary archive that documents climatic changes in the central high Andes over the last millennium and extends this perspective back to ~2500 years BP (Fig. 7).

To interpret the APA01 record within a broader climatic framework, it is necessary to briefly recall how Late Holocene climate phases such as the Medieval Climate Anomaly (MCA) and Little Ice Age (LIA) are regionally expressed in the Andes. The MCA has been characterized by warm temperatures and important changes in hydroclimate conditions in many regions of the world; this effect has also been evidenced in the Andean region. On the other hand, the LIA period over the Andes is recorded through evidence of colder temperatures and increased precipitation which in turn triggered regional glacial advances (Vuille et al., 2008; Rabatel et al., 2013; Vuille et al., 2018). It is important to note that the most recent IPCC Assessment Report (AR6, 2021) explicitly states that the terms Medieval Climate Anomaly (~950–1250 CE) and Little Ice Age (~1450–1850 CE) are not used extensively, because the timing of these episodes is not well defined and varies regionally. The IPCC emphasizes that these periods should not be considered globally synchronous climate intervals, as their definitions are largely derived from reconstructions dominated by Northern Hemisphere records. Consequently, the chronology and climatic expression of the MCA and LIA in South America differ from those observed in the Northern Hemisphere, highlighting the importance of regionally resolved paleoclimate records for interpreting Andean climate variability (IPCC, 2021; Mann et al., 2009). In this sense, the chronology of these events in South America differs from the chronology in the Northern Hemisphere (e.g., Thompson et al., 1994; Masiokas et al., 2009; Kellerhals et al., 2010; Bird et al., 2011; Jomelli et al., 2016; Apaéstegui et al., 2018). An approach underlying the link between Northern Hemisphere temperature changes and their effects on tropical hydroclimate during the MCA and LIA establishes a control of the Intertropical Convergence Zone (ITCZ) position by Northern Hemisphere temperatures. A colder (warmer) Northern Hemisphere would impel a more southerly (northerly) ITCZ. These latitudinal shifts of the ITCZ influence regional circulation patterns which, in turn, regulate moisture transport over South America (Vuille et al., 2012).

However, this scheme is only applicable if the climate changes in the Northern Hemisphere and tropical Andean regions are in phase, which is not always the case. For example, in the Quelccaya varved ice core in south-central Peru (Thompson et al., 2013), net ice accumulation shows a minimum between 1100 and 1300 CE (Fig. 7b), pointing to a late MCA, and indicates that the rate of ice accumulation increases rapidly at 1520 CE, but declines sharply at 1680 CE, 170 years before the end of the LIA in the Northern Hemisphere. A core from the Illimani glacier in Bolivia (Kellerhals et al., 2010) shows warm temperatures from 1050 to 1300

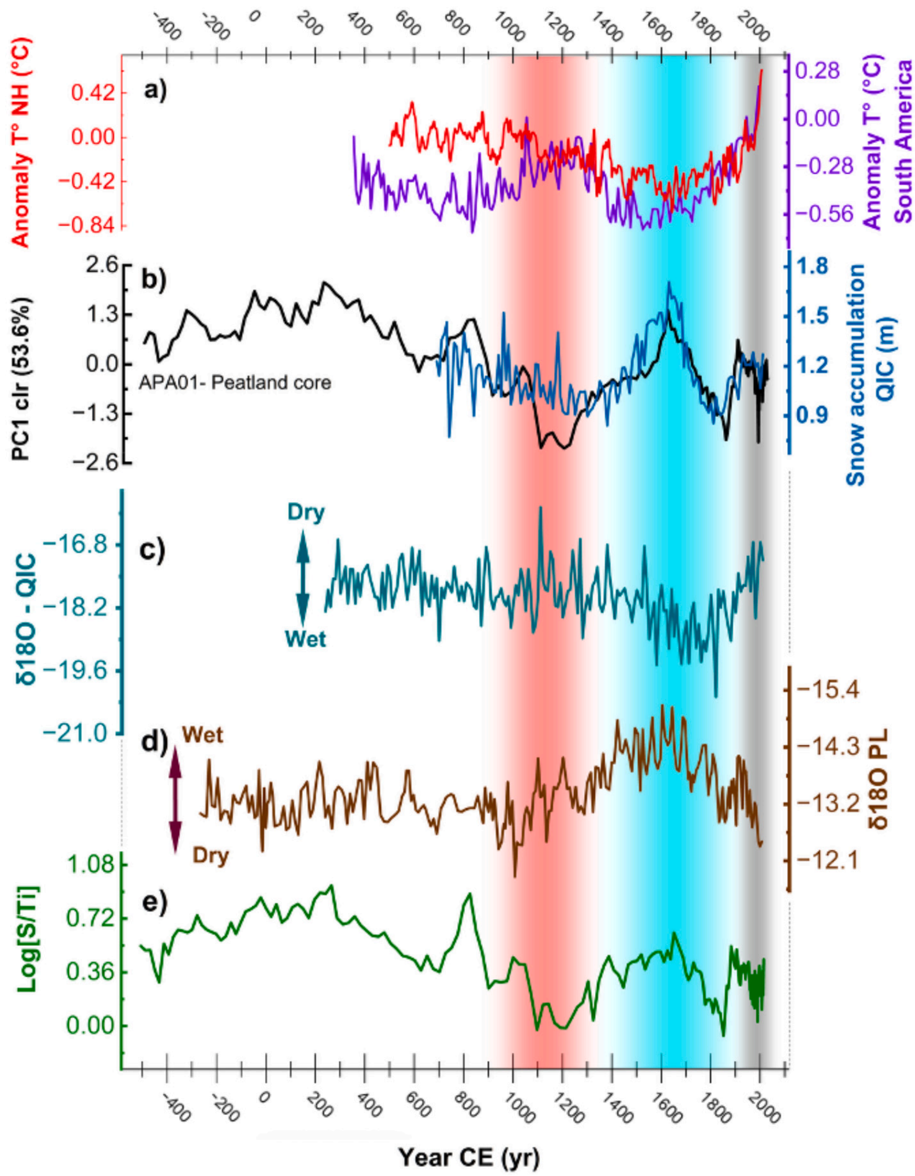

Fig. 7. Compilation of environmental and climate data over time. a) Surface temperature anomalies in the Northern Hemisphere (in red) as per Mann et al. (2009), and tropical Andes temperature anomalies from ammonium concentration in the Illimani ice core (in purple) according to Kellerhals et al. (2010). b) Superposition of the first principal component (PC1 clr) of the Andean peat core APA01 (our study), reflecting variations in organic matter production and decomposition; with the decadal mean Annual Snow Accumulation in the Quelccaya Ice Cap (Thompson et al., 2013). c) Decadal means of $\delta^{18}O$ from the Quelccaya ice core (QIC) record, again from Thompson et al. (2013), which serves as an additional climate proxy. d) $\delta^{18}O$ data from the Pumacocha lake sediment core (PL) as documented by Bird et al. (2011). e) log(S/Ti) as an indicator of the proportion of organic matter versus inorganic inputs at Apacheta. The colored bars represent the different climatological periods: the Medieval Climate Anomaly (MCA) indicated by a red bar, the Little Ice Age (LIA) by a sky-blue bar and the Current Warm Period (CWP) by a gray bar. Note that the PL record was mirrored to facilitate comparison, whereas the orientation of the QIC record is preserved as originally published. (For interpretation of the references to colour in this figure legend, the reader is referred to the web version of this article.)

CE (late MCA) and persistent cooler temperatures from 1400 to 1800 CE (Fig. 7a), marking a LIA more consistent with the northern hemisphere in terms of Illimani temperatures than Quelccaya precipitation (Fig. 7a, b). These phase shifts raise doubt about the sole control of Northern Hemisphere temperatures over Andean tropical climate currently.

To comprehend the influence of global and regional climate changes on the APA01 record, a comparison with Northern Hemisphere temperature anomaly reconstruction (Mann et al., 2009) and the temperature anomaly reconstruction obtained from the ammonium concentration in the Illimani ice core (Kellerhals et al., 2010) is shown at the top of the Fig. 7a. Note that the Illimani record also shows very different behavior from the Northern Hemisphere, before the MCA. Complementary to this finding, the Fig. 7b shows the comparison between the PC1-clr of the Apacheta record (interpreted as organic matter accumulation) and the snow accumulation reconstruction obtained from the Quelccaya ice core (Thompson et al., 2013). The strong correspondence between the two records suggests that rates of organic matter accumulation in the peat core can be related to the effective balance in tropical snow accumulation (precipitation vs sublimation) at Quelccaya, since both systems are in the same region and linked through common geographical features (high altitudes) and hydrological processes. The comparison with the log(S/Ti) obtained from the APA01 record (Fig. 7e), interpreted as a tracer of the organic matter production, indicates the dependence of the dynamic accumulation in the peat related to the major climate variations recorded in the Andes. In concordance with the regional hydroclimate changes in the Andes, the

PC1-clr record is shown against the $\delta^{18}O$ record of Lake Pumacocha (Bird et al., 2011) (Fig. 7d) interpreted as changes in the intensity of the South American Monsoon System.

During MCA (950–1250 CE globally), the PC1-clr curve shows a period of very negative values from 1050 to 1200 CE ±100, which takes place in a wide interval where PC1-clr values are negative from 900 to 1500 CE ±100 (Fig. 7b). This decrease in organic matter concentration, also reflected by the log(S/Ti) (Fig. 7e), is due to a minimum in accumulation of organic matter and a moderate increase in clastic sediments accumulation (Fig. 6c). At the same time, the $\delta^{18}O$ of the Quelccaya ice core (Fig. 7c) and especially that of Lake Pumacocha (Bird et al., 2011) show higher isotope values during this period, indicating a weakening of the South American Monsoon System although the 1050–1200 CE ±100 event is better marked at Apacheta (Fig. 7d). All these findings occur when the temperature reconstruction for South America arises values close to pre-industrial values (Fig. 7a). Therefore, this suggests that drier conditions during monsoon season and increased annual temperature are related to a decrease in organic matter accumulation in the APA01 peatland during the MCA.

On the other hand, during the LIA (1450–1850 CE globally), a peak of positive PC1-clr anomalies occurs from 1600 to 1700 CE ±100, quite in line with the maximum snow accumulation at Quelccaya, which takes place from 1580 to 1780 CE. An increase in precipitation linked to a more southerly position of the ITCZ forced by lower temperatures in the northern hemisphere (Fig. 7a) indicates a more humid climate that favored peat growth and the preservation of organic matter. This corresponds exactly to the interval of minimum temperatures in the northern hemisphere (Fig. 7a) but occurs late after the start of the LIA (~1450 CE). In contrast, the increase in log(S/Ti) at Apacheta, the decrease in Illimani temperatures and the negative excursion of $\delta^{18}O$ at Lake Pumacocha occurred earlier, starting at 1400 CE ±100 and ending at 1900 CE ±100.

Following the peak of organic matter accumulation in the APA01 peat core during LIA, climate underwent significant changes with a decrease in precipitation at Lake Pumacocha, organic matter accumulation at Apacheta and of snow accumulation at Quelccaya, indicating a drier climate at the end of the LIA around 1850 CE ±100 (Fig. 7). Since 1850 CE ±100 at Apacheta the accumulation rates of organic and mineral matter have increased markedly in parallel. This is probably a consequence of warmer temperatures (Fig. 7a) forced by anthropogenic climate change (Section 5.2.3). Importantly, the timing and duration of these Late Holocene phases within APA01 can vary depending on the proxy considered. For instance, the expression of LIA in PC1-clr curve (XRF PCA-clr) is limited to ~1600–1700 CE ±100, whereas the log(S/Ti) curve derived from the same XRF dataset indicates a broader interval ~ 1400–1900 CE ±100. This proxy dependent expression highlights that hydroclimatic phases are not strictly synchronous across indicators, even within a single archive.

5.2.2. *Pacific versus Atlantic oceans influence*

The climate of the Central Andes, and in particular precipitation, is also influenced by the Pacific Ocean. This is shown on an interannual scale by the relationship between the ENSO variability in the central Pacific, which is associated with increased precipitation over the central Andes during colder conditions (La Niña) and droughts during colder conditions (El Niño) (Sulca et al., 2018). At the mechanistic level, Pacific–Atlantic interactions over tropical South America are largely mediated by ENSO-related sea surface temperature anomalies in the tropical Pacific, which modulate the Walker circulation and large scale atmospheric circulation and convection over the Andes. On interannual and, to some extent, decadal (Segura et al., 2016) timescales, El Niño conditions tend to weaken the South American Monsoon System (SAMS) by reducing easterly moisture transport from the tropical Atlantic and Amazon basin toward the central Andes, whereas La Niña conditions generally enhance monsoon intensity and moisture advection. These ENSO-driven atmospheric reorganizations provide a physical framework to explain asynchronous hydroclimatic responses between the Pacific margin and the central Andes, even under similar large-scale ITCZ configurations (Garreaud et al., 2009; Vuille et al., 2012; Marengo et al., 2012).

In the sediments off Pisco, southern Peru, on the Pacific coast of South America (Salvatteci et al., 2014), the MCA is characterized by wetter conditions from 1050 to 1150 yrs. CE, whereas this interval corresponds to drier conditions at Apacheta (Fig. 8). The end of the LIA is well marked in cores from the Peruvian margin off Callao and Pisco (12°S and 14°S, respectively) by an abrupt shift toward the intensification of the Humboldt Current system and associated upwelling (Sifeddine et al., 2008, Gutirrez et al., 2009, Salvatteci et al., 2014). This rapid expansion of upwelling led to present-day high biological productivity and coincided with reduced detrital input (Fig. 8), interpreted as reduced precipitation on the western Andes linked to cooler sea surface temperatures (SST). According to the authors this shift was likely driven by a northward migration of the Intertropical Convergence Zone (Fig. 8) and the South Pacific Subtropical High to their present-day locations, coupled with a strengthening of Walker circulation, toward the end of the Little Ice Age (Sifeddine et al., 2008, Gutirrez et al., 2009, Salvatteci et al., 2014). This abrupt change has been dated by ^{210}Pb to ~1820 CE, most likely corresponds to the sudden increase in PC1 at Apacheta, indicating, in contrast to the Peruvian margin records, a shift toward wetter conditions that cannot be explained solely by a northward displacement of the ITCZ. During the Current Warm Period, the upwellings of the Humboldt system remain very active, while in the Andes, glacier retreat has been continuous since the end of the Little Ice Age (e.g., Jomelli et al., 2009). This reduction in the ice-covered surface area leads to a decrease in albedo and contributes to the difference in climate change between the Central Pacific margin and the Central Andes.

Overall, the contrasting hydroclimatic signals recorded along the central Peruvian Pacific margin and in the central Andes highlight that Andean precipitation variability cannot be explained solely by meridional shifts of the ITCZ. Instead, the combined influence of Pacific-driven atmospheric circulation changes, particularly through ENSO-related modulation of the South American Monsoon System, provides a coherent framework to account for the asynchronous responses observed between coastal and high-Andean records during the last 2500 years (Fig. 8).

5.2.3. *Climatic and anthropogenic control on clastic supply*

The greatest input of clastic mineral material into the basin is observed during dry periods in the Apacheta peatland sediments. Changes in precipitation phase (rainfall vs. snowfall) and event intensity could have influenced erosion. Precipitation at these elevations (>3600 m a.s.l.), occurs as solid forms (snow), particularly during the cold season and associated frost events (SENAMHI, 2020). Snow is also observed during the warm monsoon season when rainfalls occurred at night as stratiform precipitation while liquid rainfall occurred during the afternoon as convective precipitation (Perry et al., 2013). A reduction in snow precipitation and an increase of convective precipitation under a warmer climate may explain the increase of soil erosion.

In addition to hydroclimatic forcing, anthropogenic land use also plays a key role in soil erosion. High Andean peatlands have historically been exposed to grazing by camelids (llamas, alpacas). This reduces protective vegetation cover, compacts the soil, and exacerbates slope erosion, facilitating the transport of clastic into the basin even with sporadic rainfall (Schittek et al., 2015; Yager et al., 2021). During dry periods, grazing pressure concentrates on bofedales, as they act as forage refuges (Chepstow-Lusty et al., 2009). The case of Apacheta shows that increased erosion during dryer and warmer periods is not restricted to glacial valleys (Vergara et al., 2024) but is the result of the interaction between climatic conditions (seasonality, type and shifts of precipitation) and land use. In recent decades (approx. 1995–2015), the decrease in organic matter (Fig. S1c) is consistent with a scenario of degradation driven both by warming, which favors decomposition (Hribljan et al.,

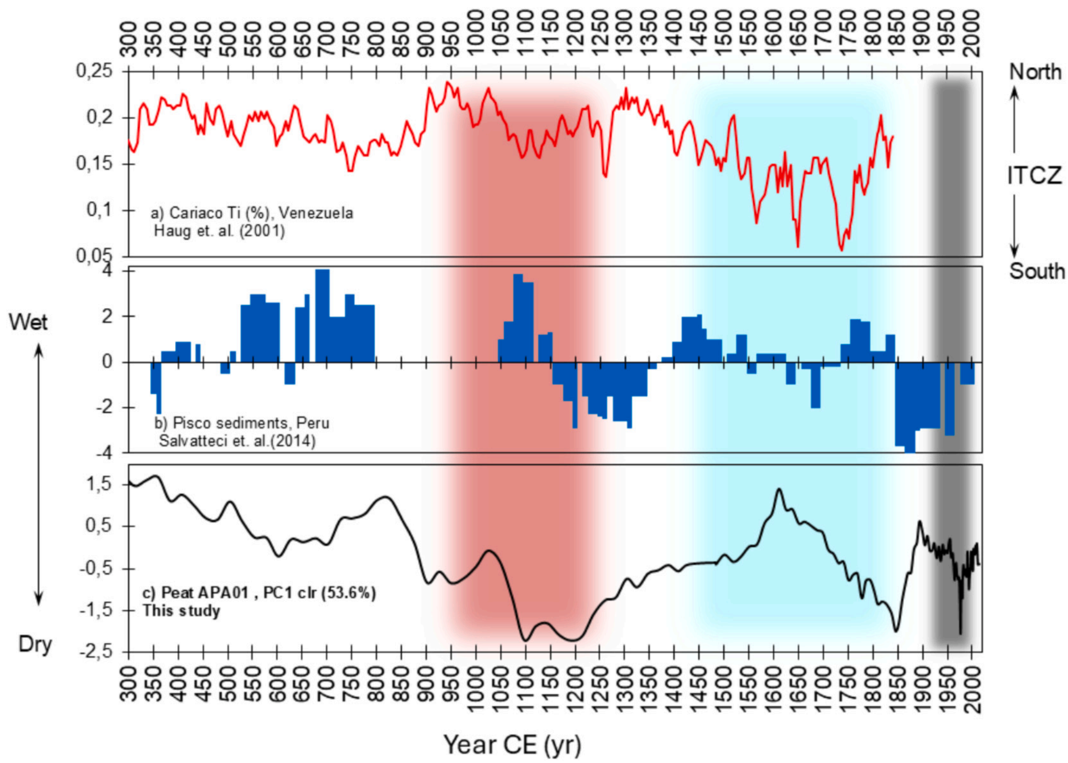

Fig. 8. Atlantic-Pacific controls on Central Andean hydroclimate (300 – ~2010 CE). (a) Cariaco Basin, Venezuela: 3-point average of Ti (%) record (Haug et al., 2001), limited to the common interval (300 – ~2010 CE), interpreted as a proxy for ITCZ latitudinal shifts. (b) Peruvian margin off Pisco (14° S), average terrigenous runoff index derived from standardized Al and Ti values (Z-scores) (Salvatteci et al., 2014); positive values indicate increased precipitation on the western Andean slope, while negative values denote drier conditions. (c) Apacheta peatland (APA01), PC1-clr (Z; 53.6% of the variance) obtained using XRF-scanner (this study), reflecting variations in organic matter production (positive values) and decomposition (negative values). The colored bars represent different climatological periods: the Medieval Climate Anomaly (MCA), indicated by a red bar; the Little Ice Age (LIA), by a light blue bar; and the Current Warm Period (CWP), by a gray bar. (For interpretation of the references to colour in this figure legend, the reader is referred to the web version of this article.)

2014, 2024), and by the cumulative impact of grazing, which alters soil hydrology and stability.

6. Conclusions

Although the process of organic material accumulation in the peatland is not strictly a sedimentary process, since it involves the growth of the plants that make up the peat, it can nevertheless be studied using sedimentological methods. The chronological consistency of the AMS ^{14}C dates, which show no age reversals, together with the calibration of the modern period using post-bomb (pMC) data. This chronological framework enables a reliable synchronization between the PC1-clr (representing organic matter dynamics) and Quelccaya ice cap accumulation record, indicating the sensitivity of the APA01 archive to regional hydroclimatic variability.

The close temporal correspondence between PC1-clr and Quelccaya accumulation indicates that organic matter content and production in the peatland are strongly linked to regional changes in the precipitation–evaporation balance. Furthermore, our study highlights that high altitude Andean archives function as complex systems where different geochemical proxies can exhibit distinct temporal sensitivities to the same climatic forcing. These internal phase offsets emphasize the importance of multi proxy approach to capture the full range of peatland responses during major intervals such as the Little Ice Age (LIA).

Comparison with other tropical Andean records, such as the Illimani glacier and lake Pumacocha, supports the occurrence of drier Medieval Climate Anomaly (MCA) and wetter conditions during the LIA in the region. However, the observed discrepancies between tropical Andean climate phases and Northern Hemisphere temperature variations indicated that local climate does not depend solely on Northern Hemisphere forcing via shifts in the Intertropical Convergence Zone (ITCZ). Additional processes, including variability in Pacific sea surface temperatures (SST), probably play a key role modulating regional climate conditions.

Finally, our analysis of the Apacheta peatland core indicates that wet periods, such as the central phase of the Little Ice Age, are conducive to the accumulation of organic matter. Conversely, dry periods favor the deposition of mineral material resulting from watershed erosion. The current marked decline in peat organic matter accumulation observed on the APA01 is highly concerning under ongoing warming. Given their role in carbon storage and water regulation, continued monitoring and improved understanding of peatlands responses to climate change are essential for anticipating ecosystems vulnerability and informing conservation strategies.

CRediT authorship contribution statement

Yizet E. Huaman-Navarro: Writing – review & editing, Writing – original draft, Visualization, Validation, Methodology, Investigation, Formal analysis, Data curation. **Bruno Turcq:** Writing – review & editing, Writing – original draft, Visualization, Validation, Supervision, Resources, Methodology, Investigation, Formal analysis, Data curation. **Patricia Moreira-Turcq:** Writing – review & editing, Writing – original draft, Visualization, Supervision, Resources, Project administration, Investigation, Funding acquisition, Formal analysis, Data curation, Conceptualization. **James Apaéstegui:** Writing – review & editing, Investigation. **Jorge Luis Garcia:** Writing – review & editing, Software. **Isabelle Billy:** Writing – review & editing, Data curation. **Romina Llanos:** Writing – review & editing, Visualization, Investigation. **Bram Willems:** Writing – review & editing, Resources, Funding acquisition.

Declaration of competing interest

The authors declare that they have no known competing financial interests or personal relationships that could have appeared to influence the work reported in this paper.

Acknowledgments

We express our sincere gratitude to Swan Zerathe for valuable discussions regarding the presence of glaciers in the study area. This research was funded by the Institut de Recherche pour le Développement (IRD, France) and the USAID Partnership for Enhanced Engagement in Research (PEER) program through the projects: “Strengthening resilience of Andean River basin headwaters facing global change” (PGA - 084063) and “AGUA - ANDES: Ecological Infrastructure Strategies for Enhancing Water Sustainability in the Semi-Arid Andes” (PGA – 174194). Additional support was provided by the French National Program EC2CO-BIOHEFECT. Y. Huaman-Navarro's fellowship is generously supported by PRONABEC-Peru.

Appendix A. Supplementary data

Supplementary data to this article can be found online at https://doi.org/10.1016/j.palaeo.2026.113775.

Data availability

Data for this study are available from the corresponding author upon request.

References

Aitchison, J., 1982. The statistical analysis of compositional data. J. R. Stat. Soc. B. Methodol. 44 (2), 139–160. https://doi.org/10.1111/J.2517-6161.1982.TB01195.X.

Aitchison, J., Greenacre, M., 2002. Biplots of compositional data. J. R. Stat. Soc.: Ser. C: Appl. Stat. 51 (4), 375–392. https://doi.org/10.1111/1467-9876.00275.

Ancapichún, S., De Pol-Holz, R., Christie, D.A., Santos, G.M., Collado-Fabbri, S., Garreaud, R., Lambert, F., Orfanoz-Cheuquelaf, A., Rojas, M., Southon, J., Turnbull, J.C., Creasman, P.P., 2021. Radiocarbon bomb-peak signal in tree-rings from the tropical Andes register low latitude atmospheric dynamics in the southern hemisphere. Sci. Total Environ. 774, 145126. https://doi.org/10.1016/J.SCITOTENV.2021.145126.

Apaéstegui, J., Cruz, F.W., Sifeddine, A., Vuille, M., Espinoza, J.C., Guyot, J.L., Khodri, M., Strikis, N., Santos, R.V., Cheng, H., Edwards, L., Carvalho, E., Santini, W., 2014. Hydroclimate variability of the northwestern Amazon basin near the Andean foothills of Peru related to the South American monsoon system during the last 1600 years. Clim. Past 10 (6), 1967–1981. https://doi.org/10.5194/cp-10-1967-2014.

Apaéstegui, J., William, F., Vuille, M., Fohlmeister, J., 2018. Precipitation changes over the eastern Bolivian Andes inferred from speleothem (δ18O) records for the last 1400 years. Earth Planet. Sci. Lett. 494 (May), 124–134. https://doi.org/10.1016/j.epsl.2018.04.048.

Bábek, O., Fačevicová, K., Žídek, M., Sedláček, J., Muehlmann, C., Nordhausen, K., Hron, K., 2022. X-ray fluorescence scanning of soft and wet-sediment cores in terrestrial environments; a robust blind source separation approach. J. Geochem. Explor. 243. https://doi.org/10.1016/J.GEXPLO.2022.107106.

Bain, D.C., 1976. A titanium-rich soil clay. J. Soil Sci. 27 (1), 68–70. https://doi.org/10.1111/J.1365-2389.1976.TB01976.X.

Banríon, M., Cobelli, M., Crowley, Q.G., 2023. Applying machine learning to model radon using topsoil geochemistry. Appl. Geochem. 158, 105790. https://doi.org/10.1016/J.APGEOCHEM.2023.105790.

Benavides, J.C., 2015. The effect of drainage on organic matter accumulation and plant communities of high-altitude peatlands in the Colombian tropical Andes. Mire Peat 15, 1–15.

Benavides, J.C., Rocha, S., Blanco, E.A., 2023. Spatial and temporal patterns of methane emissions from mountain peatlands in the northern Andes across a disturbance gradient. Front. Earth Sci. 11, 1078830. https://doi.org/10.3389/feart.2023.1078830.

Benfield, A.J., Yu, Z., Benavides, J.C., 2021. Environmental controls over holocene carbon accumulation in Distichia muscoides-dominated peatlands in the eastern Andes of Colombia. Quat. Sci. Rev. 251, 106687. https://doi.org/10.1016/J.QUASCIREV.2020.106687.

Bird, B.W., Abbott, M.B., Vuille, M., Rodbell, D.T., Stansell, N.D., Rosenmeier, M.F., 2011. A 2,300-year-long annually resolved record of the South American summer monsoon from the Peruvian Andes. Proc. Natl. Acad. Sci. USA 108, 8583–8588. https://doi.org/10.1073/pnas.1003719108.

Blaauw, M., 2010. Methods and code for 'classical' age-modelling of radiocarbon sequences. Quat. Geochronol. 5, 512–518. https://doi.org/10.1016/j.quageo.2010.01.002.

Bronk Ramsey, C., 2020. OxCal 4.4. Radiocarbon 62, 1–25. https://doi.org/10.1017/RDC.2020.59.

Buytaert, W., Célleri, R., De Bièvre, B., Cisneros, F., Wyseure, G., Deckers, J., Hofstede, R., 2006. Human impact on the hydrology of the Andean páramos. Earth Sci. Rev. 79 (1–2), 53–72. https://doi.org/10.1016/J.EARSCIREV.2006.06.002.

Carballeira, R., Pontevedra-Pombal, X., 2020. Diatoms in paleoenvironmental studies of peatlands. Quaternary 2020 3 (2), 10. https://doi.org/10.3390/QUAT3020010.

Chepstow-Lusty, A.J., Frogley, M.R., Bauer, B.S., Leng, M.J., Boessenkool, K.P., Carcaillet, C., Ali, A.A., Gioda, A., 2009. Putting the rise of the Inca Empire within a climatic and land management context. Clim. Past 5, 375–388. https://doi.org/10.5194/cp-5-375-2009.

Chimner, R.A., Karberg, J.M., 2008. Long-term carbon accumulation in two tropical mountain peatlands, Andes mountains, Ecuador. Mire Peat 3, 04.

Cooper, D.J., Wolf, E.C., Colson, C., Vering, W., Granda, A., Meyer, M., 2010. Alpine peatlands of the Andes, Cajamarca, Peru. Arct. Antarct. Alp. Res. 42 (1), 19–33. https://doi.org/10.1657/1938-4246-42.1.19.

Cooper, D.J., Kaczynski, K., Slayback, D., Yager, K., 2018. Growth and organic carbon production in peatlands dominated by Distichia muscoides, Bolivia, South America. Arct. Antarct. Alp. Res. 47 (3), 505–510. https://doi.org/10.1657/AAAR0014-060.

Croudace, I., Rindby, A., Rothwell, R., 2006. ITRAX: Description and evaluation of a new multi-function X-ray core scanner. Geol. Soc. London Spec. Publ. https://doi.org/10.1144/GSL.SP.2006.267.01.04.

Croudace, I.W., Löwemark, L., Tjallingii, R., Zolitschka, B., 2019a. Current perspectives on the capabilities of high resolution XRF core scanners. Quat. Int. 514, 5–15. https://doi.org/10.1016/J.QUAINT.2019.04.002.

Croudace, I.W., Löwemark, L., Tjallingii, R., Zolitschka, B., 2019b. High resolution XRF core scanners: a key tool for the environmental and palaeoclimate sciences. Quat. Int. 514, 1–4. https://doi.org/10.1016/J.QUAINT.2019.05.038.

Cuesta, F., Llambí, L.D., Huggel, C., Drenkhan, F., Gosling, W.D., Muriel, P., Jaramillo, R., Tovar, C., 2019. New land in the neotropics: a review of biotic community, ecosystem, and landscape transformations in the face of climate and glacier change. Reg. Environ. Chang. 19 (6), 1623–1642. https://doi.org/10.1007/S10113-019-01499-3.

Dickens, G.R., 2011. Climate of the Past Down the Rabbit Hole: Toward Appropriate Discussion of Methane Release from Gas Hydrate Systems during the Paleocene-Eocene Thermal Maximum and Other Past Hyperthermal Events, 7, pp. 831–846. https://doi.org/10.5194/cp-7-831-2011.

Domic, A.I., Capriles, J.M., Meneses, R.I., Pacheco, P., 2021. Plant community assembly is predicted by an environmental gradient in high-altitude wetlands in the semiarid western Bolivian Andes. Mire Peat 27, 12. https://doi.org/10.19189/MaP.2019.JSP.StA.1916.

Earle, L.R., Warner, B.G., Aravena, R., 2003. Rapid development of an unusual peat-accumulating ecosystem in the chilean altiplano. Quat. Res. 59 (1), 2–11. https://doi.org/10.1016/S0033-5894(02)00011-X.

Fennell, J., Bentley, L.R., 1998. Distribution of sulfate and organic carbon in a prairie till setting: Natural versus industrial sources. Water Resour. Res. 34 (7), 1781–1794. https://doi.org/10.1029/98WR00827.

Filzmoser, P., Hron, K., Reimann, C., 2009. Principal component analysis for compositional data with outliers. Environmetrics 20 (6), 621–632. https://doi.org/10.1002/ENV.966.

Fonkén, M.M., 2014. An introduction to the bofedales of the Peruvian high Andes. Mire Peat 15, 05.

Gaiser, E., Rühland, K., 2010. Diatoms as indicators of environmental change in wetlands and peatlands. In: The Diatoms: Applications for the Environmental and Earth Sciences, Second Edition, pp. 473–496. https://doi.org/10.1017/CBO9780511763175.026.

Garreaud, R.D., Vuille, M., Compagnucci, R., Marengo, J., 2009. Present-day South American climate. Palaeogeogr. Palaeoclimatol. Palaeoecol. 281 (3–4), 180–195. https://doi.org/10.1016/j.palaeo.2007.10.032.

Giráldez, L., Silva, Y., Zubieta, R., Sulca, J., 2020. Change of the rainfall seasonality over central peruvian Andes: onset, end, duration and its relationship with large-scale atmospheric circulation. Climate 8, 23. https://doi.org/10.3390/cli8020023.

Gribbin, T., Mackay, J.D., MacDonald, A., Hannah, D.M., Buytaert, W., Baiker, J.R., Montoya, N., Perry, L.B., Seimon, A., Rado, M., Arias, S., Vargas, M., 2024. Bofedal wetland and glacial melt contributions to dry season streamflow in a high-Andean headwater watershed. Hydrol. Process. 38 (8), 1–21. https://doi.org/10.1002/hyp.15237.

Grunsky, E.C., Caritat, P. de, 2020. State-of-the-art analysis of geochemical data for mineral exploration. Geochem.: Explor., Environ., Anal. 20 (2), 217–232. https://doi.org/10.1144/geochem2019-031.

Gutiérrez-Salazar, M., Medrano-Vizcaíno, P., 2019. The effects of climate change on decomposition processes in Andean Páramo ecosystems: a systematic review. Appl. Ecol. Environ. Res. 17, 4957–4970. https://doi.org/10.15666/aeer/1702_49574970.

Gutirrez, D., Sifeddine, A., Field, D.B., Ortlieb, L., Vargas, G., Chavez, F.P., Velazco, F., Ferreira, V., Tapia, P., Salvatteci, R., Boucher, H., Morales, M.C., Valdes, J., Reys, J. L., Campusano, A., Bous Safir, M., Mandeng-Yogo, M., Garca, M., Baumgartner, T., 2009. Rapid reorganization in ocean biogeochemistry off Peru towards the end of the little ice age. Biogeosciences 6 (5), 835–848. https://doi.org/10.5194/bg-6-835-2009.

Hammer, Ø., Harper, D.A.T., Ryan, P.D., 2001. PAST: paleontological statistics software package for education and data analysis. Palaeontol. Electron. 4 (1) [PAST 4.15]: 9pp.

Haug, G.H., Hughen, K.A., Sigman, D.M., Peterson, L.C., Röhl, U., 2001. Southward migration of the intertropical convergence zone through the holocene. Science 293 (5533), 1304–1308. https://doi.org/10.1126/science.1059725.

Hogg, A.G., Heaton, T.J., Hua, Q., Palmer, J.G., Turney, C.S., Southon, J., Wacker, L., 2020. SHCal20 southern hemisphere calibration, 0–55,000 years cal BP. Radiocarbon 62 (4), 759–778. https://doi.org/10.1017/RDC.2020.59.

Hribljan, J., Cooper, D., Sueltenfuss, J., Wolf, E.C., Heckman, K., Lilleskov, E., Chimner, R., 2014. Carbon storage and long-term rate of accumulation in high-altitude Andean peatlands of Bolivia. Mires and Peat 15, 1–14.

Hribljan, J.A., Suárez, E., Heckman, K.A., et al., 2016. Peatland carbon stocks and accumulation rates in the Ecuadorian páramo. Wetl. Ecol. Manag. 24, 113–127. https://doi.org/10.1007/s11273-016-9482-2.

Hribljan, J.A., Hough, M., Lilleskov, E.A., et al., 2024. Elevation and temperature are strong predictors of long-term carbon accumulation across tropical Andean mountain peatlands. Mitig. Adapt. Strateg. Glob. Chang. 29 (1). https://doi.org/10.1007/s11027-023-10089-y.

Hua, Q., Turnbull, J.C., Santos, G.M., Rakowski, A.Z., Ancapichún, S., De Pol-Holz, R., Turney, C.S.M., 2022. Atmospheric radiocarbon for the period 1950–2019. Radiocarbon 64 (4), 723–745. https://doi.org/10.1017/RDC.2021.95.

INAIGEM, 2018. Inventario Nacional de Glaciares/Las Cordilleras Glaciares del Perú 2018. Instituto Nacional de Investigación en Glaciares y Ecosistemas de Montaña, Huaraz. https://hdl.handle.net/20.500.12748/57.

INAIGEM, 2023. Inventario Nacional de Glaciares y Lagunas de Origen Glaciar 2023. Instituto Nacional de Investigación en Glaciares y Ecosistemas de Montaña, Huaraz. https://hdl.handle.net/20.500.12748/499.

IPCC, 2021. Climate Change 2021: The Physical Science Basis. Contribution of Working Group I to the Sixth Assessment Report of the Intergovernmental Panel on Climate Change [Masson-Delmotte, V., P. Zhai, A. Pirani, S.L. Connors, C. Péan, S. Berger, N. Caud, Y. Chen, L. Goldfarb, M.I. Gomis, *M. Huang*, K. Leitzell, E. Lonnoy, J.B.R. Matthews, T.K. Maycock, T. Waterfield, O. Yelekçi, R. Yu, and B. Zhou (eds.)]. Cambridge University Press, Cambridge, United Kingdom and New York, NY, USA. https://doi.org/10.1017/9781009157896, 2391 pp.

Jansen, J.H.F., Van Der Gaast, S.J., Koster, B., Vaars, A.J., 1998. CORTEX, a shipboard XRF-scanner for element analyses in split sediment cores. Mar. Geol. 151 (1–4), 143–153. https://doi.org/10.1016/S0025-3227(98)00074-7.

Jomelli, V., Favier, V., Rabatel, A., Brunstein, D., Hoffmann, G., Francou, B., 2009. Fluctuations of glaciers in the tropical Andes over the last millennium and palaeoclimate implications: a review. Palaeogeogr. Palaeoclimatol. Palaeoecol. 281 (3–4), 269–282. https://doi.org/10.1016/j.palaeo.2008.10.033.

Jomelli, V., Lane, T., Favier, V., Masson-Delmotte, V., Swingedouw, D., Rinterknecht, V., Schimmelpfennig, I., Brunstein, D., Verfaillie, D., Adamson, K., Leanni, L., Mokadem, F., Aumaître, G., Bourlès, D.L., Keddadouche, K., 2016. Paradoxical cold conditions during the medieval climate anomaly in the western Arctic. Sci. Rep. 2016 6 (1), 1–9. https://doi.org/10.1038/srep32984.

Kellerhals, T., Brütsch, S., Sigl, M., Knüsel, S., Gäggeler, H.W., Schwikowski, M., 2010. Ammonium concentration in ice cores: a new proxy for regional temperature reconstruction? J. Geophys. Res. Atmos. 115, 1–8. https://doi.org/10.1029/2009JD012603.

Kern, O.A., Koutsodendris, A., Mächtle, B., Christanis, K., Schukraft, G., Scholz, C., Kotthoff, U., Pross, J., 2019. XRF core scanning yields reliable semiquantitative data on the elemental composition of highly organic-rich sediments: evidence from the Füramoos peat bog (Southern Germany). Sci. Total Environ. 697, 134110. https://doi.org/10.1016/J.SCITOTENV.2019.134110.

King, C., Michelutti, N., Meyer-Jacob, C., Bindler, R., Tapia, P., Grooms, C., Smol, J.P., 2021. Diatoms and other siliceous indicators track the ontogeny of a "bofedal" (wetland) ecosystem in the Peruvian Andes. Botany 99 (8), 491–505. https://doi.org/10.1139/cjb-2020-0196.

Kock, S.T., Schittek, K., Mächtle, B., Wissel, H., Maldonado, A., Lücke, A., 2019a. Late holocene environmental changes reconstructed from stable isotope and geochemical records from a cushion-plant peatland in the Chilean Central Andes (27°S). J. Quat. Sci. 34 (2), 153–164. https://doi.org/10.1002/jqs.3088.

Kock, S.T., Schittek, K., Lücke, A., Maldonado, A., Mächtle, B., 2019b. Geomorphodynamics as recorded in a high-andean cushion peatland of the western chilean Central Andes (27°S) during the last 1800 cal. Yr BP. Zeitschrift Fur Geomorphologie 62 (June), 183–205. https://doi.org/10.1127/zfg_suppl/2019/0537.

Kokfelt, U., Struyf, E., Randsalu, L., 2009. Diatoms in peat – dominant producers in a changing environment? Soil Biol. Biochem. 41 (8), 1764–1766. https://doi.org/10.1016/J.SOILBIO.2009.05.012.

Kylander, M.E., Martínez-Cortizas, A., Bindler, R., Kaal, J., Sjöström, J.K., Hansson, S.V., Silva-Sánchez, N., Greenwood, S.L., Gallagher, K., Rydberg, J., Mörth, C.M., Rauch, S., 2018. Mineral dust as a driver of carbon accumulation in northern latitudes. Sci. Rep. 8 (1), 1–10. https://doi.org/10.1038/s41598-018-25162-9.

Lee, A.S., Huang, J.J.S., Burr, G., Kao, L.C., Wei, K.Y., Liou, S.Y.H., 2019. High resolution record of heavy metals from estuary sediments of Nankan river (Taiwan) assessed by rigorous multivariate statistical analysis. Quat. Int. 527, 44–51. https://doi.org/10.1016/J.QUAINT.2018.11.018.

Liu, K., Reese, C.A., Thompson, L.G., 2005. Ice-core pollen record of climatic changes in the central Andes during the last 400 yr. Quat. Res. 64, 272–278. https://doi.org/10.1016/j.yqres.2005.06.001.

Liu, K., Reese, C.A., Thompson, L.G., 2007. A potential pollen proxy for ENSO derived from the Sajama ice core. Geophys. Res. Lett. 34, 1–5. https://doi.org/10.1029/2006GL029018.

Loisel, J., Gallego-Sala, A.V., Amesbury, M.J., Magnan, G., Anshari, G., Beilman, D.W., Benavides, J.C., Blewett, J., Camill, P., Charman, D.J., Chawchai, S., Hedgpeth, A., Kleinen, T., Korhola, A., Large, D., Mansilla, C.A., Müller, J., van Bellen, S., West, J. B., Wu, J., 2021. Expert assessment of future vulnerability of the global peatland carbon sink. Nat. Clim. Chang. 11 (1), 70–77. https://doi.org/10.1038/s41558-020-00944-0.

Longman, J., Veres, D., Wennrich, V., 2019. Utilisation of XRF core scanning on peat and other highly organic sediments. Quat. Int. 514 (October 2018), 85–96. https://doi.org/10.1016/j.quaint.2018.10.015.

Löwemark, L., Chen, H.F., Yang, T.N., Kylander, M., Yu, E.F., Hsu, Y.W., Lee, T.Q., Song, S.R., Jarvis, S., 2011. Normalizing XRF-scanner data: a cautionary note on the interpretation of high-resolution records from organic-rich lakes. J. Asian Earth Sci. 40 (6), 1250–1256. https://doi.org/10.1016/j.jseaes.2010.06.002.

Lücke, A., Kock, S., Wissel, H., Kulemeyer, J.J., Lupo, L.C., Schäbitz, F., Schittek, K., 2022. Hydroclimatic record from an Altiplano cushion peatland (24°S) indicates large-scale reorganisation of atmospheric circulation for the late holocene. PLoS One 17 (11), e0277027. https://doi.org/10.1371/JOURNAL.PONE.0277027.

Maldonado, M., Maldonado-Ocampo, J.A., Ortega, H., Encalada, A.C., Carvajal-Vallejos, F.M., Rivadeneira, J.F., Acosta, F., Jacobsen, D., Crespo-Pérez, V., Rivera, C., 2007. Biodiversity in aquatic systems of the tropical Andes. In: Herzog, S. K., Martínez, R., Jørgensen, P.M., Tiessen, H. (Eds.), Climate Change and Biodiversity in the Tropical Andes (pp. 276–294). Inter-American Institute for Global Change Research (IAI) & Scientific Committee on Problems of the Environment (SCOPE).

Mann, M.E., Zhang, Z., Rutherford, S., Bradley, R.S., Hughes, M.K., Shindell, D., Ammann, C., Faluvegi, G., Ni, F., 2009. Global signatures and dynamical origins of the little ice age and medieval climate anomaly. Science 326 (5957), 1256–1260. https://doi.org/10.1126/science.1177303.

Marengo, J.A., Liebmann, B., Grimm, A.M., Misra, V., Silva Dias, P.L., Cavalcanti, I.F.A., Carvalho, L.M.V., Berbery, E.H., Ambrizzi, T., Vera, C.S., Saulo, A.C., Nogues-Paegle, J., Zipser, E., Seth, A., 2012. Recent developments on the South American monsoon system. Int. J. Climatol. 32 (1), 1–21. https://doi.org/10.1002/joc.2254.

Martínez-Amigo, V., Jaramillo, R., 2024. Cushion plants from the Andes — an overview of current knowledge and some research needs. Wetland Sci. Pract. January 97–103. https://doi.org/10.1672/UCRT083-616.

Masiokas, M.H., Rivera, A., Espizua, L.E., Villalba, R., Delgado, S., Carlos, J., 2009. Glacier fluctuations in extratropical South America during the past 1000 years. Palaeogeogr. Palaeoclimatol. Palaeoecol. 281 (3–4), 242–268. https://doi.org/10.1016/j.palaeo.2009.08.006.

McCarter, C.P.R., Rezanezhad, F., Quinton, W.L., Gharedaghloo, B., Lennartz, B., Price, J., Connon, R., Van Cappellen, P., 2020. Pore-scale controls on hydrological and geochemical processes in peat: Implications on interacting processes. Earth Sci. Rev. 207, 103227. https://doi.org/10.1016/J.EARSCIREV.2020.103227.

McKinley, J.M., Grunsky, E., Mueller, U., 2018. Environmental monitoring and peat assessment using multivariate analysis of regional-scale geochemical data. Math. Geosci. 50, 235–246. https://doi.org/10.1007/s11004-017-9686-x.

Monge-Salazar, M.J., Tovar, C., Cuadros-Adriazola, J., Baiker, J.R., Montesinos-Tubée, D. B., Bonnesoeur, V., Antiporta, J., Román-Dañobeytia, F., Fuentealba, B., Ochoa-Tocachi, B.F., Buytaert, W., 2022. Ecohydrology and ecosystem services of a natural and an artificial bofedal wetland in the Central Andes. Sci. Total Environ. 838, 155968. https://doi.org/10.1016/J.SCITOTENV.2022.155968.

Moreno, A., Giralt, S., Valero-Garcés, B., Sáez, A., Bao, R., Prego, R., Pueyo, J.J., González-Sampériz, P., Taberner, C., 2007. A 14 kyr record of the tropical Andes: the lago chungará sequence (18°S, northern Chilean Altiplano). Quat. Int. 161 (1), 4–21. https://doi.org/10.1016/j.quaint.2006.10.020.

Mosquera, G.M., Célleri, R., Lazo, P.X., Vaché, K.B., Perakis, S.S., Crespo, P., 2016. Combined use of isotopic and hydrometric data to conceptualize ecohydrological processes in a high-elevation tropical ecosystem. Hydrol. Process. 30 (17), 2930–2947. https://doi.org/10.1002/HYP.10927.

Nikonova, L., Kurganova, I., Lopes De Gerenyu, V., Rogova, O., Golovatskaya, E., 2023. Impact of temperature and moisture on the decomposition of peat-forming plants: results of a two-year incubation experiment. Forests. https://doi.org/10.3390/f14122355.

Oyague, E., 2020. Peatlands of the Central Andes Puna, South America. Wetland Sci. Pract. 37 (4), 255–260. https://doi.org/10.1672/ucrt083-204.

Oyague, E., Cooper, D.J., Ingol, E., 2022. Effects of land use on the hydrologic regime, vegetation, and hydraulic conductivity of peatlands in the central Peruvian Andes. J. Hydrol. 609 (February), 127687. https://doi.org/10.1016/j.jhydrol.2022.127687.

Perez, N., Loisel, J., 2023. Synthesis of high-Andean peat cores reveals suite of holocene climate conditions favorable for peat formation. Quat. Sci. Rev. 322 (August), 108413. https://doi.org/10.1016/j.quascirev.2023.108413.

Perry, L.B., Seimon, A., Kelly, G.M., 2013. Precipitation delivery in the tropical high Andes of southern Peru: new findings and paleoclimatic implications. Int. J. Climatol. 34 (1), 197–215. https://doi.org/10.1002/joc.3679.

Polk, M.H., Young, K.R., Baraer, M., Mark, B.G., Mckenzie, J.M., Bury, J., Carey, M., 2017. Exploring hydrologic connections between tropical mountain wetlands and glacier recession in Peru's Cordillera Blanca. Appl. Geogr. 78, 94–103. https://doi.org/10.1016/j.apgeog.2016.11.004.

Polk, M.H., Young, K.R., Cano, A., León, B., 2019. Vegetation of Andean wetlands (bofedales) in Huascarán National Park, Peru. Mire Peat 24, 1–26. https://doi.org/10.19189/MaP.2018.SNPG.387.

Rabatel, A., Francou, B., Soruco, A., Gomez, J., Cáceres, B., Ceballos, J.L., Basantes, R., Vuille, M., Sicart, J.E., Huggel, C., Scheel, M., Lejeune, Y., Arnaud, Y., Collet, M., Condom, T., Consoli, G., Favier, V., Jomelli, V., Galarraga, R., Wagnon, P., 2013. Current state of glaciers in the tropical Andes: a multi-century perspective on glacier evolution and climate change. Cryosphere 7 (1), 81–102. https://doi.org/10.5194/tc-7-81-2013.

Rothwell, R.G., Croudace, I.W., 2015. Micro-XRF Studies of Sediment Cores: A Perspective on Capability and Application in the Environmental Sciences, pp. 1–21. https://doi.org/10.1007/978-94-017-9849-5_1.

Salvatteci, R., Gutiérrez, D., Field, D., Sifeddine, A., Ortlieb, L., Bouloubassi, I., Boussafir, M., Boucher, H., Cetin, F., 2014. The response of the Peruvian upwelling ecosystem to centennial-scale global change during the last two millennia. Clim. Past 10 (2), 715–731. https://doi.org/10.5194/cp-10-715-2014.

Schittek, K., Forbriger, M., Mächtle, B., Schäbitz, F., Wennrich, V., Reindel, M., Eitel, B., 2015. Holocene environmental changes in the highlands of the southern peruvsian Andes (14° s) and their impact on pre-Columbian cultures. Clim. Past 11, 27–44. https://doi.org/10.5194/cp-11-27-2015.

Schittek, K., 2012. Cushion peatlands ("bofedales") in the central Andes - high-resolution archives for palaeoenvironmental studies. Quaternary International 279–280 (2012), 434. https://doi.org/10.1016/j.quaint.2012.08.1414.

Schittek, K., Kock, S.T., Lücke, A., Hense, J., Ohlendorf, C., Kulemeyer, J.J., Lupo, L.C., Schäbitz, F., 2016. A high-altitude peatland record of environmental changes in the NW Argentine Andes (24° S) over the last 2100 years. Clim. Past 12 (5), 1165–1180. https://doi.org/10.5194/cp-12-1165-2016.

Schittek, K., Forbriger, M., Berg, D., Hense, J., Schäbitz, F., Eitel, B., 2018. Last millennial environmental dynamics in the western Peruvian Andes inferred from the development of a cushion-plant peat hillock. Perspect. Plant Ecol. Evol. Syst. 30 (September 2017), 115–124. https://doi.org/10.1016/j.ppees.2017.09.002.

Schittek, K., Wowrek, J., Käuffer, N., Reindel, M., Mächtle, B., 2025. Solar forcing as driver for late holocene rainfall intensity in the Peruvian Andes. Quat. Int. 718 (August 2024). https://doi.org/10.1016/j.quaint.2024.109647.

Segura, H., Espinoza, J.C., Junquas, C., Takahashi, K., 2016. Evidencing decadal and interdecadal hydroclimatic variability over the Central Andes. Environ. Res. Lett. 11 (9). https://doi.org/10.1088/1748-9326/11/9/094016.

Segura, H., Espinoza, J.C., Junquas, C., Lebel, T., Vuille, M., Garreaud, R., 2020. Recent changes in the precipitation-driving processes over the southern tropical Andes/western Amazon. Clim. Dyn. 54 (5–6), 2613–2631. https://doi.org/10.1007/S00382-020-05132-6.

SENAMHI, 2020. CLIMAS DEL PERÚ – Mapa de Clasificación Climática Nacional. https://www.senamhi.gob.pe/load/file/01404SENA-4.pdf.

Sifeddine, A., Gutiérrez, D., Ortlieb, L., Boucher, H., Velazco, F., Field, D., Vargas, G., Boussafir, M., Salvatteci, R., Ferreira, V., García, M., Valdés, J., Caquineau, S., Mandeng Yogo, M., Cetin, F., Solis, J., Soler, P., Baumgartner, T., 2008. Laminated sediments from the central peruvian continental slope: a 500-year record of upwelling system productivity, terrestrial runoff and redox conditions. Prog. Oceanogr. 79 (2–4), 190–197. https://doi.org/10.1016/j.pocean.2008.10.024.

Skrzypek, G., Engel, Z., Chuman, T., Šefrna, L., 2011. Distichia peat - a new stable isotope paleoclimate proxy for the Andes. Earth Planet. Sci. Lett. 307 (3–4), 298–308. https://doi.org/10.1016/j.epsl.2011.05.002.

Smol, J.P., Stoermer, E.F., 2010. The diatoms: applications for the environmental and earth sciences. In: The Diatoms: Applications for the Environmental and Earth Sciences, Second Edition, pp. 1–667. https://doi.org/10.1017/CBO9780511763175.

Sulca, J., Takahashi, K., Espinoza, J.C., Vuille, M., Lavado-Casimiro, W., 2018. Impacts of different ENSO flavors and tropical pacific convection variability (ITCZ, SPCZ) on austral summer rainfall in South America, with a focus on Peru. Int. J. Climatol. 38 (1), 420–435. https://doi.org/10.1002/joc.5185.

Thompson, L.G., Davis, M.E., Mosley-Thompson, E., 1994. Glacial records of global climate: a 1500-year tropical ice core record of climate. Hum. Ecol. 22 (1), 83–95. https://doi.org/10.1007/BF02168764.

Thompson, L.G., Mosley-Thompson, E., Davis, M.E., Zagorodnov, V.S., Howat, I.M., Mikhalenko, V.N., Lin, P.N., 2013. Annually resolved ice core records of tropical climate variability over the past ~1800 years. Science (New York, N.Y.) 340 (6135), 945–950. https://doi.org/10.1126/science.1234210.

Tribovillard, N., Algeo, T.J., Lyons, T., Riboulleau, A., 2006. Trace metals as paleoredox and paleoproductivity proxies: an update. Chem. Geol. 232 (1–2), 12–32. https://doi.org/10.1016/J.CHEMGEO.2006.02.012.

Vergara, I., Garreaud, R., Delaney, I., Ayala, Á., 2024. Deglaciation in the subtropical Andes has led to a peak in sediment delivery. Commun. Earth Environ. 5 (1), 1–7. https://doi.org/10.1038/s43247-024-01815-8.

Verzijl, A., Quispe, S.G., 2013. The system nobody sees: irrigated wetland management and alpaca herding in the Peruvian Andes. Mt. Res. Dev. 33 (3), 280–293. https://doi.org/10.1659/MRD-JOURNAL-D-12-00123.1.

Vimeux, F., Ginot, P., Schwikowski, M., Vuille, M., Hoffmann, G., Thompson, L.G., Schotterer, U., 2009. Climate variability during the last 1000 years inferred from Andean ice cores: a review of methodology and recent results. Palaeogeogr. Palaeoclimatol. Palaeoecol. 281 (3–4), 229–241. https://doi.org/10.1016/j.palaeo.2008.03.054.

Vuille, M., Kaser, G., Juen, I., 2008. Glacier mass balance variability in the Cordillera Blanca, Peru and its relationship with climate and the large-scale circulation. Glob. Planet. Chang. 62 (1–2), 14–28. https://doi.org/10.1016/j.gloplacha.2007.11.003.

Vuille, M., Burns, S.J., Taylor, B.L., Cruz, F.W., Bird, B.W., Abbott, M.B., Kanner, L.C., Cheng, H., Novello, V.F., 2012. Climate of the past. In: A Review of the South American Monsoon History as Recorded in Stable Isotopic Proxies over the Past Two Millennia, 8, pp. 1309–1321. https://doi.org/10.5194/cp-8-1309-2012.

Vuille, M., Rabatel, A., Jacobsen, D., 2018. Rapid decline of snow and ice in the tropical Andes-impacts, uncertainties and challenges ahead. Earth-Sci. Rev. 176 (November 2017), 195–213. https://doi.org/10.1016/j.earscirev.2017.09.019.

Wang, J.P., Wang, X.J., Zhang, J., 2013. Evaluating Loss-on-Ignition method for determinations of soil organic and inorganic carbon in arid soils of northwestern China. Pedosphere 23 (5), 593–599. https://doi.org/10.1016/S1002-0160(13)60052-1.

Wang, L., Liu, B., McKinley, J.M., Cooper, M.R., Li, C., Kong, Y., Shan, M., 2021. Compositional data analysis of regional geochemical data in the Lhasa area of Tibet, China. Appl. Geochem. 135, 105108. https://doi.org/10.1016/J.APGEOCHEM.2021.105108.

Weltje, G.J., Tjallingii, R., 2008. Calibration of XRF core scanners for quantitative geochemical logging of sediment cores: theory and application. Earth Planet. Sci. Lett. 274 (3–4), 423–438. https://doi.org/10.1016/j.epsl.2008.07.054.

Weltje, G.J., Bloemsma, M.R., Tjallingii, R., Heslop, D., Röhl, U., Croudace, I.W., 2015. Prediction of Geochemical Composition from XRF Core Scanner Data: A New Multivariate Approach Including Automatic Selection of Calibration Samples and Quantification of Uncertainties, August, pp. 507–534. https://doi.org/10.1007/978-94-017-9849-5_21.

Yager, K., Prieto, M., Meneses, R.I., 2021. Reframing pastoral practices of Bofedal management to increase the resilience of Andean water towers. Mt. Res. Dev. 41, A1–A9. https://doi.org/10.1659/MRD-JOURNAL-D-21-00011.1.